

Electronic Thesis and Dissertation Repository

2-11-2019 10:30 AM

The impact-generated hydrothermal system of the East Clearwater Lake impact structure, Quebec, Canada

Derek King
The University of Western Ontario

Supervisor
Osinski, Gordon R.
The University of Western Ontario

Graduate Program in Geology
A thesis submitted in partial fulfillment of the requirements for the degree in Master of Science
© Derek King 2019

Follow this and additional works at: <https://ir.lib.uwo.ca/etd>



Part of the [Geology Commons](#), and the [Other Earth Sciences Commons](#)

Recommended Citation

King, Derek, "The impact-generated hydrothermal system of the East Clearwater Lake impact structure, Quebec, Canada" (2019). *Electronic Thesis and Dissertation Repository*. 6144.
<https://ir.lib.uwo.ca/etd/6144>

This Dissertation/Thesis is brought to you for free and open access by Scholarship@Western. It has been accepted for inclusion in Electronic Thesis and Dissertation Repository by an authorized administrator of Scholarship@Western. For more information, please contact wlsadmin@uwo.ca.

The impact-generated hydrothermal system of the East Clearwater Lake impact structure, Quebec, Canada

Abstract

Alteration mineralization at impact craters gives insight into the hydrothermal system generated post-impact. This is the first work to document the alteration mineralization to characterize the East Clearwater impact-generated hydrothermal system. The East Clearwater hydrothermal system in the impact melt rocks and melt-bearing breccias transitions from zeolite-smectite assemblages to chlorite-dominant assemblages with depth. pH evolution of the East Clearwater impact-generated hydrothermal system reflects magmatic-driven hydrothermal systems in granitic rocks. West Clearwater has a different alteration style. Given an impact forms a hydrothermal system, the style of alteration will not only vary dependent on target lithologies (i.e., crystalline, sedimentary, mixed target), but also due to paleogeographic setting (i.e., costal, shallow marine, intracontinental). The impact-generated hydrothermal system of East Clearwater contains millerite, vaesite-pyrite, and galena due to a percentage of impactor imparted into the melt. Given ideal impact velocities do not completely vapourize an impactor, alteration products, especially metals, can influence secondary mineralization.

Keywords

East Clearwater, impact-generated hydrothermal system, hydrothermal, impact crater, alteration, secondary mineralization, Clearwater, West Clearwater, zeolite, chlorite, sulfide, clinoptilolite, heulandite, clinoptilolite-Ca, heulandite-Ca millerite, vaesite, galena, sphalerite.

Acknowledgments

Thanks to: Marc Beauchamp for assistance with the microprobe; Tianqi Xie for helping with the Raman; Alex Rupert for aiding with in-situ XRD. Peter Christoffersen for assistance with the ASD spectrometer; Dr. Livio Tornabene with guidance for spectral analysis; Dr. Phil McCausland for general advice and thesis discussion; Dr. Richard Grieve for insight into East Clearwater; Dr. Gordon Osinski for guiding me and ensuring I had a project; my parents for all of their unconditional support; and to all my friends that I have made at Western University over the past 2 years.

Table of Contents

The impact-generated hydrothermal system of the East Clearwater Lake impact structure, Quebec, Canada	i
Abstract.....	i
Acknowledgments.....	ii
Table of Contents.....	iii
List of Tables (where applicable)	v
List of Figures (where applicable).....	vi
Chapter 1.....	1
1 Introduction and Literature Review	1
1.1 Impact Craters.....	1
1.1.1 Impacts and Earth	4
1.1.2 Impact Cratering Mechanics.....	5
1.2 Impact-generated Hydrothermal systems	11
1.2.1 Heat sources	11
1.2.2 Fluid Sources	12
1.2.3 Porosity and permeability	12
1.2.4 Alteration Setting.....	13
1.3 Outro	15
Bibliography	17
Chapter 2.....	23
2 Impact-generated hydrothermal system at East Clearwater.....	23
2.1 Introduction.....	23
2.2 Wiyâshâkimî (Clearwater Lake) Complex	23
2.2.1 Loups Marins Suite (Alma1 & Alma2)	26
2.2.2 Desbergères Suite (Adeb).....	27

2.2.3	Châteauguay Suite (Achg)	27
2.2.4	Impactites	28
2.2.5	Previous Noted Alteration.....	29
2.3	Methods.....	29
2.3.1	Samples	29
2.3.2	Analytical methods	30
2.4	Results.....	31
2.4.1	Zone 1	31
2.4.2	Zone 2	44
2.5	Discussion.....	48
2.5.1	Heat Sources	48
2.5.2	Fluid sources	48
2.5.3	Early Stage	48
2.5.4	Main Stage pH and temperature constraints	49
2.5.5	Comparison with other impact-generated hydrothermal systems.....	51
2.5.6	The significance of millerite and vaesite-pyrite.....	53
2.5.7	Conclusions.....	53
	Bibliography	54
	Chapter 3.....	58
3	Conclusions.....	58
	Curriculum Vitae	60

List of Tables (where applicable)

Table 1: Ni-Fe Sulfide WDS. Millerite and Vaesite-pyrite. b.d. indicates “below detection”.	33
Table 2: Geochemistry of the Pb-Zn-Cu-Fe sulfides. b.d. indicates “below detection”.....	36
Table 3: Clinoptilolite-Ca and heulandite-Ca in Zone 1. Clinoptilolite-Ca has a $T_{Si} \geq 80$ and an $Si:Al \geq 4$. Heulandite-Ca has a $T_{Si} < 80$ and an $Si:Al < 4$ (Coombs et al., 1997; Coombs et al., 1998).	39
Table 4: Geochemical data from clinoptilolite-Ca and heulandite-Ca in Zone 1 at 271.2 m depth. *H ₂ O was assumed as the remaining mass (100-total) **Total value not including H ₂ O.	41

List of Figures (where applicable)

Figure 1: Galileo's observation of the cratered lunar surface (Galilei, 1610).....	3
Figure 2: The first three stages of impact crater conception. Modified from Osinski and Pierazzo, 2012.....	8
Figure 3: Impact-generated hydrothermal deposits found at typical complex craters. From Osinski et al., 2013.....	14
Figure 4: Landsat image of the Clearwater Lakes. Modified from (Landsat 8, 2013).	24
Figure 5. The Geology of the East Clearwater crater complex. From youngest to oldest: Tramont Suite (Atra), Maurel Suite (Amau), Qullinaaraaluk Suite (Aluk), Loups Marins Suite (Cpx-bearing is Alma1; Opx-bearing is Alma2), Desbergères Suite (Adeb), Lesdiguières/Favard Suite (Ald/Afav), Châteauguay Suite (Achg), Sem suite (Asem), and Coursolles Suite (Acou). Modified from (Simard et al., 2008).	26
Figure 6: A. Upper Zone 1. section from the impact melt-bearing breccia at 271.6 m (sample 948.5). B. Lower Zone 1. Vesicular impact melt rock. 279.4 m (sample 2-63-978). C. Zone 2. Fine-grained coherent impact melt rock. 308.7 m (sample 1089).	29
Figure 7: Millerite (Mlr) and vaesite-pyrite (Va-Py). Millerite is acicular and radiates out from a point. Vaesite-pyrite is octahedral and moderately altered.	33
Figure 8: Red Oxidation Halo emanating from millerite (Mlr) and vaesite-pyrite at 271.2 m depth. A. Oxidation halos visible from the top of the melt sheet. The red box indicates the location of images B-D in this figure B. PPL image of the alteration haloes. They are inside clinoptilolite-Ca (Cpt-Ca) crystals. C. XPL image showing the tabular nature of the clinoptilolite-Ca. Two points of nucleation are present. D. BSE reveals the millerite at the centre of the alteration halo on the left. There appears to be none in the one on the right.	34
Figure 9: The Pb-Zn-Cu-Fe group of sulfides found at East Clearwater at 271.2 m depth. A. Reflected light image of a large sphalerite (Sp) with other sulfides encased in it. The white box indicates the location of B in this figure. B. A section of A showing all four sphalerite,	

galena (Gn), chalcopyrite (Ccp), and pyrite (Py). C&D. Plane polarized light and back scattered electron image showing the botryoidal heulandite-Ca (Hul-Ca), respectively.....	35
Figure 10: μ XRD of zeolites at 271.2 m depth. XRD scan with both clinoptilolite-Ca and heulandite-Ca for reference.....	37
Figure 11: Raman Spectroscopy of zeolites at 271.2 m depth. Measured Raman peaks, closely resembling the signatures of both clinoptilolite-Ca and heulandite-Ca.	38
Figure 12: Radial clinoptilolite-Ca (Cpt-Ca) and botryoidal heulandite-Ca (Hul-Ca). A. Scanning electron image highlights the radial nature, indicated by the red arrows, of the tabular clinoptilolite-Ca. B. Element map of strontium. The botryoidal heulandite-Ca contains a higher amount of strontium. C. Plane polarized light image centred on the oxidation halo. The oxidation of the nickel-iron sulfides is evident (millerite and vaesite-pyrite) encased in the radial heulandite. D. Silica over aluminum element map. The different zeolites are highlighted by Si:Al ratios. Quartz (Qtz) is highlighted amongst the botryoidal heulandite.....	40
Figure 13: UV-Vis-NIR spectroscopy of Zone 1 and 2 compared to smectites.	42
Figure 14: Radial clinoptilolite-Ca (Cpt-Ca), botryoidal heulandite-Ca (Hul-Ca), and rim heulandite-Ca at 271.6 m depth A. Composite image highlighting the presence of galena (Gn) and the structure of the zeolites. B. Elemental map of strontium. Higher concentrations are also apparent in the rim heulandite-Ca. C. Magnesium element map. Mg-rich saponite (Sap) is found in the botryoidal structures surrounded by heulandite-Ca. D. Silica over Aluminum element map. Si:Al highlights the difference between the two zeolites.....	43
Figure 15: The mineralization style of vugs in the chlorite zone. A) Radial quartz (Qtz) in a vug at 280.1 m depth. B) Chlorite (Chl) infilling vug with magnetite (Mgt) found in a clast at 290.4 m. C & D) Quartz dominated vug with chlorite, biotite (Bt), and pyrite (Py) at 295.3 m.	45
Figure 16: A. Large Pentlandite crystal at 308.9 m depth. Galena (Gn) exsolution in pentlandite (Pn), precipitation of sphalerite (Sp) and pyrite (Py) on the rim. B. Zoned calcite (Cal) with quartz (Qtz). The lighter shades are caused by higher Mn and Fe.	46

Figure 17: Mineralization with depth in East Clearwater Core 2-63. Black means minerals have been identified. Dashed lines indicate trace amounts. Units from top to bottom: Impact melt-bearing breccia; Vesicular impact melt rock; Fine-grained coherent impact melt rock. Zones from top to bottom: Zone 1; Zone 2. Zones are defined by the transition between the zeolites and clays and the chlorite. 47

Figure 18: The formation of minerals over the temperature of the East Clearwater hydrothermal system. 51

Chapter 1

1 Introduction and Literature Review

Hydrothermal systems can be an important post-impact process in both simple and complex impact craters. Such systems are controlled by the heat sources (e.g., geothermal gradient uplift, shock heating, and melt generation), fluid availability, and porosity and permeability due to shocked, fractured rocks and impactites. A hydrothermal system redistributes elements throughout the pathways it travels. This hydrothermal history can be seen through alteration mineral assemblages in vugs and veins present in lithologies in and around the impact crater. Alteration mineral assemblages can give insight into the temperature, longevity, pH, and reduction potential of the impact-generated hydrothermal system.

1.1 Impact Craters

The first documentation of impact craters occurred in 1610, when Galileo published his observations of the lunar landscape (Figure 1) (Galilei, 1610). In 1794, the idea that meteorites, specifically pallasites, were projectiles from space that formed fireballs in the sky as they fell contributed even more to the planetary sciences (Chladni, 1794). In 1893, it was proposed that the craters observed on the Moon may not be from volcanic processes, but must be formed from impact events (Gilbert, 1893). The first impact crater to be proposed on Earth was Barringer, or Meteor Crater in the early 1900s (Barringer, 1905), although it was not accepted as fact by the scientific community. The general consensus amongst astronomers was that the lunar craters were giant volcanoes, and out of the few who theorized them to be impact craters, even fewer could fathom the Earth's surface contained scars from celestial objects (Melosh, 1989). Planetary science would remain on the fringe until the 1960s, when interest in space rocketed astronomically. Barringer Crater was accepted as an impact crater with the discovery of the first natural occurrence of coesite, a high-pressure polymorph of silica formed at pressures only attained during impacts and nuclear tests (Chao et al., 1960). The realization of impact craters as an important planet-forming geological process commenced with the

development of shock metamorphic criteria (French and Short, 1968) and the Space Age interest in space exploration dominantly via the Apollo Missions (Osinski and Pierazzo, 2012).



Figure 1: Galileo's observation of the cratered lunar surface (Galilei, 1610).

1.1.1 Impacts and Earth

Currently, 193 craters have been discovered on and under Earth's surface (Impact Earth, 2018), yet >380,000 impact craters with diameter ≥ 1 km have been discovered on Mars (Robbins and Hynes, 2012). Earth has a diameter that is just under twice the size of Mars (Carr et al., 1980). Theoretical models have predicted that there may still be a few (~ 90) small-sized (1–6 km) impacts that have not yet been discovered on Earth (Hergarten and Kenkmann, 2015). However, overall it is not the lack of discovery, but the hydrology, atmosphere, and distribution that significantly reduces the number of impact craters observed on Earth.

The persistent weathering process by the Earth's hydrological cycle rapidly erodes impact craters over geological time. Smaller impact craters are lost more quickly due to weathering. For example, exposed impact structures of < 20 km in diameter are recognizable for < 600 Ma (Grieve and Robertson, 1979). Whereas impact craters with diameters of ~ 90 km can survive over geological timespans (~ 3 Ga) in absence of any unique geological circumstances (e.g., tectonism) (Grieve and Robertson, 1979; Johnson and Bowling, 2014). Smaller craters that are protected by overlying sedimentary units will be preserved so long as the cover is not removed (Grieve and Robertson, 1979).

Earth's atmosphere interferes with impacting bodies. Many celestial bodies (e.g., the Moon, Ceres) lack any significant atmosphere to interact with projectiles. On the lunar surface, meteoroid-sized impactors require a few kilometres per second velocity to shock melt the target lunar regolith (Ahrens and O'Keefe, 1972). On Earth, stony objects > 50 m and iron bodies > 20 m pass through the atmosphere with negligible effects on acceleration, amongst other deformations (Osinski and Pierazzo, 2012). These projectiles are affected by the full gravitational acceleration of the Earth and strike with the square root of the sum of the escape velocity of the Earth squared and the cosmic velocity of the projectile squared (French, 1998).

$$\vec{V}_{impact} = \sqrt{\vec{V}_{escape}^2 + \vec{V}_{cosmic}^2}$$

Anything smaller than mentioned above, such as meteoroids, or loosely-consolidated projectiles will be negatively accelerated, deformed, ablated, and generally disrupted while passing through the atmosphere traversing towards the surface (Passey and Melosh, 1980; Bland and Artemieva, 2003; Collins et al., 2012). Given a small projectile doesn't completely burn up in the atmosphere, it will lose enough velocity resulting in metre-sized, shockwave-lacking penetration craters (Osinski and Pierazzo, 2012).

Impacts craters only form on land and in shallow marine settings. Land cover on Earth is ~29% of the surface and the continental shelf covers ~7% of the Earth (National Research Council (US), 1979). These percentages have fluctuated over geological time, but most recorded impacts would have occurred under similar enough conditions (Kominz, 2001; Durack et al., 2012). Areas that are tectonically stable over geological time better preserve impact craters. Naturally, the majority of impacts are found in the Northern hemisphere (due to the larger land surface area) in the geologically stable North American and European cratons (Grieve and Robertson, 1979). Confirmed craters can be skewed by socioeconomics. Stable countries with well-funded geology programs, exploration, and academic institutions tend to find more craters and contain more individuals seeking them out (Grieve and Robertson, 1979).

1.1.2 Impact Cratering Mechanics

Impact craters form when a hypervelocity projectile (e.g., comet, asteroid) impacts into a larger target body. Both objects collide in a spatial sense, but the larger target constrains what occurs to the smaller projectile due to conservation of momentum (Melosh, 1989). After the impact, complex mechanisms produce an impact crater. There are three stages that constitute impact crater production and modification (Figure 2). Hydrothermal alteration can be considered as a 4th stage. These stages overlap and range from milliseconds to hundreds to thousands of years after impact (Gault et al., 1968; Gault et al., 1974; Melosh, 1989; Osinski and Pierazzo, 2012):

- (1) Contact and compression: the transfer of kinetic energy from impactor to target via a compressive shockwave;
- (2) Excavation: the resulting excavation of the crater from complex interactions;

- (3) Modification: Post-impact modification of the impact basin by geologic processes; and
- (4) Alteration: chemical and physical alteration through hydrothermal processes of the entire crater complex (Kirsimäe and Osinski, 2012; Osinski and Pierazzo, 2012; Osinski et al., 2013).

1.1.2.1 Contact and Compression

An impact commences when the projectile contacts the surface of the target. The exception is bodies with atmospheres (see above, 1.1.1). Different compositions (i.e., porous cometary, stony, and iron) of impactors have quantitative and qualitative differences when connecting with the silicate surface of a planetary body.

The pressure at the point of impact is comparable to a nuclear bomb; a stony or iron projectile with a velocity of 15–20 kms^{-1} will produce a sound-barrier breaking, compressive shockwave radiating pressures of several hundred GPa and temperatures exceeding 10,000 K (Shoemaker, 1959; Shoemaker, 1960; Grieve et al., 1977; Shoemaker, 1977; Collins et al., 2012). This shockwave is the boundary between high pressure, compressed material and uncompressed target rock (Figure 2). As the shockwave propagates, a rarefaction wave follows. The rarefaction wave is the boundary between the high-pressure zone and the low-pressure zone (Figure 2) (Ahrens and O’Keefe, 1972; Melosh, 1989). The increase in energy from shock compression and subsequent rarefaction is sufficient to induce shock metamorphism, melting, and/or vapourization of target material close to the point of impact (Ahrens and O’Keefe, 1972; Grieve et al., 1977; Osinski and Pierazzo, 2012).

Due to the resistivity of the target rocks, part of the shockwave is reflected into the negatively accelerating projectile, producing the highest shock pressures during the impact process (Ahrens and O’Keefe, 1972). The shockwave propagates through the impactor and is reflected as a rarefaction or tensile wave at the impactor-atmosphere boundary (Ahrens and O’Keefe, 1972). As this rarefaction wave propagates into the impactor, it unloads the shock pressure, resulting in the melting and vapourizing of the projectile (Gault et al., 1968; Melosh, 1989; Osinski and Pierazzo, 2012). The projectile

will only penetrate 1 to 2 times its diameter before it unloads all of its kinetic impact energy into the target rock (Kieffer and Simonds, 1980; O'Keefe and Ahrens, 1982). Once the projectile is completely unloaded, the contact and compression stage ends (Melosh, 1989).

1.1.2.2 Excavation

The transition between the contact and compression stage and the excavation stage is a continuum (Figure 2) (Melosh, 1989; Osinski and Pierazzo, 2012). Excavation is a reaction to both the shockwaves and rarefaction waves from the contact and compression stage and is a relatively low pressure, large-scale deformation and flow of target material (Croft, 1980). The impact crater is opened by interactions with the shockwave and the target rock, as pressure approaches zero after the shockwave passes and particle velocity drops to about $1/5^{\text{th}}$ the peak velocity of the shock wave (Melosh, 1985; Melosh and Ivanov, 1999). The projectile is no longer contributing energy into the system (Osinski and Pierazzo, 2012).

The shockwave continues to radiate out hemispherically from the deepest point impacted and into the surrounding target rock, decreasing in pressure with distance (Figure 2) (Melosh, 1989). The projectile is now in a very different physical and chemical state and the rarefaction wave that was that originated from the impactor-atmosphere boundary travels into the target sequence (Melosh, 1989; Osinski and Pierazzo, 2012). The combination of the rarefaction wave and hemispherical shockwaves results in 1) in shock melting from target lithologies unloading (Ahrens and O'Keefe, 1972; Grieve et al., 1977; Osinski and Pierazzo, 2012); 2) formation of a near-surface zone of interference (Dence, 1968; Dence et al., 1977; Croft, 1980; Grieve and Cintala, 1981; Melosh, 1989), and 3) formation of a transient crater from excavation and displacement of target material (Dence, 1968; Dence et al., 1977; Croft, 1980; Grieve and Cintala, 1981; Melosh, 1989).

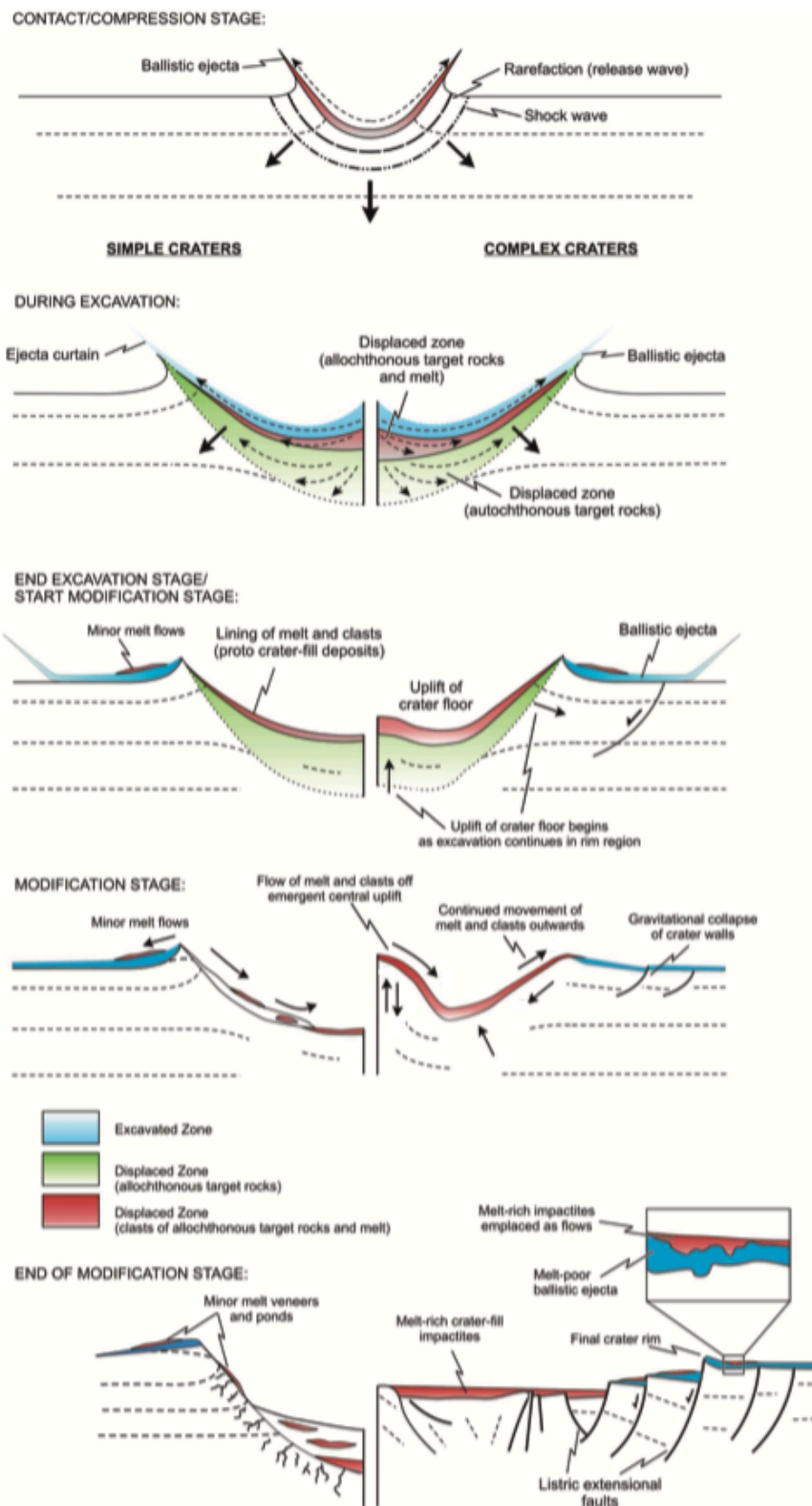


Figure 2: The first three stages of impact crater conception. Modified from Osinski and Pierazzo, 2012.

Shock melting occurs in all impacts. On the lunar surface, silicate impactors with velocities of 7–12 kms^{-1} are able to vapourize quartz and periclase. Silicate and iron impactors with velocities of 3–4 kms^{-1} are able to induce shock melting in basaltic and diabasic soils (similar to lunar regolith) (Ahrens and O’Keefe, 1972). Iron meteorites impacting at speed from 4–6 kms^{-1} are able to induce shock melting in quartz, plagioclase, olivine, and pyroxene (Ahrens and O’Keefe, 1972). Melt at impact craters is found as ejecta, impact melt-bearing breccias, and impact melt sheets that line the crater floor (Grieve et al., 1977). Impacts into sedimentary and mixed targets produce carbonate and siliceous melt, whereas impacts in crystalline targets produce almost exclusively siliceous melt (Osinski et al., 2018). Sedimentary targets have significantly larger volatile contents, which escape readily and contribute to hydrothermal systems post- crater formation (Kieffer and Simonds, 1980).

It is suggested material from the top third of the transient crater is ballistically ejected and material in the bottom two-thirds is mostly displaced within the transient crater (Stöffler et al., 1975). A mixture of melt and rock debris form a lining of the transient cavity (French, 1998; Osinski and Pierazzo, 2012). However, material from the bottom two-thirds can be transported in a second episode of ejecta emplacement consisting of melt-rich ground flows at the terminus of excavation and into the modification stage (Osinski et al., 2011). During the second ejecta emplacement, high-velocity melt will flow or eject over the transient cavity rim and melt with lower velocities remain in the transient crater (Grieve et al., 1977; Osinski et al., 2011; Osinski and Pierazzo, 2012). Eventually the shockwaves and rarefaction waves become so weak that they no longer excavate or displace any more material, and excavation ends (French, 1998; Osinski and Pierazzo, 2012).

1.1.2.3 Modification

The transition between excavation and modification is a continuum, as parts of the crater commence modification while excavation continues elsewhere (Figure 2). The extent of modification is determined by the parent body, size of the transient crater, and the target lithologies (Melosh, 1989; Melosh and Ivanov, 1999; Osinski and Pierazzo, 2012). The depth of the transient cavity depends on the impactor depth. The diameter of the transient

crater is about three times its depth (Maxwell, 1977; Croft, 1985; French, 1998). The appearance of the final crater is largely dependent on the size of the impact, and planetary gravity. There are two different types of craters observed on Earth that get their final appearance during modification: 1) simple craters and 2) complex craters.

Simple craters are bowl-like depression with only minor uplift and other almost negligible modifications to the transient crater (Figure 2) (Dence, 1965; Grieve et al., 1977; Melosh, 1989; Osinski and Pierazzo, 2012). Complex craters possess a central uplift, an annular trough, and an outer faulted rim (Figure 2) (Dence, 1965; Grieve, 1991; Grieve and Therriault, 2004). The type of impact crater is affected by the gravitational field of the parent body. Higher gravitational fields result in lower transitional boundary between simple and complex craters from higher gravitational acceleration (Melosh, 1989). On Earth, simple craters generally have diameters $< \sim 2\text{--}4$ km and complex craters have diameters $> \sim 2\text{--}4$ km. The target lithologies can affect the morphology and morphometry of the crater, with boundaries between simple and complex craters being ~ 2 km in sedimentary targets and ~ 4 km in crystalline targets (Osinski and Pierazzo, 2012).

Complex craters form when the transient crater is gravitationally unstable (Dence, 1965). This results in the central uplift of the transient crater, and collapse of the transient crater to form a shallower, gravitationally stable crater geomorphology (Quaide et al., 1965; Grieve, 1991; Osinski and Pierazzo, 2012). The maximum stratigraphic central uplift possible is about one tenth the final crater diameter (Ivanov et al., 1982; Melosh, 1989). The central uplift of the transient crater floor exposes lithologies from below the crater floor creating a surrounding annular trough (Dence, 1965; Osinski and Pierazzo, 2012). The uplift of rocks elevates the geothermal gradient, creating a second thermal anomaly with a geothermal gradient on the order of $100\text{ }^{\circ}\text{Ckm}^{-1}$ (Naumov, 2005). The temperature increase in the central uplift is on the orders of $100\text{--}200\text{ }^{\circ}\text{C}$ in impact craters with diameters of $\sim 20\text{--}30$ km to $< 1000\text{ }^{\circ}\text{C}$ in impact craters on the scale of hundreds of kilometres in diameter (Grieve et al., 1977; Ivanov, 2004; Kirsimäe and Osinski, 2012).

Less deformed breccias on the crater walls form terraces that slump into the annular trough, interlayering with materials inside the crater and ejecta. This results in an intermixture of impact breccia and melt inside the crater (Dence, 1965; Grieve et al., 1977; Melosh, 1989; Grieve, 1991; Osinski and Pierazzo, 2012).

1.2 Impact-generated Hydrothermal systems

Impact-generated hydrothermal systems are an important process that effects the physical, chemical, and even biological properties of an impact crater. Hydrothermal alteration is known to be associated with over 70 craters on Earth (Naumov, 2002; Naumov, 2005; Osinski et al., 2013). Many studies have been done on impact-generated hydrothermal systems (e.g., Newsom, 1980; Daubar and Kring, 2001; Osinski et al., 2001; Naumov, 2002; Hode et al., 2003; Osinski et al., 2004; Abramov and Kring, 2005; Naumov, 2005; Osinski, 2005; Pirajno, 2009; Osinski et al., 2013; Sapers et al., 2016).

Hydrothermal systems are the redistribution of mass and energy through thermal, chemical, and mechanical processes caused by circulating H₂O fluids and molecular diffusion (Norton, 1984). H₂O fluid circulation stabilizes chemical differences and occurs due to the difference in entropy between a heat source and its cooler surroundings (Norton, 1984). Impact-generated hydrothermal systems are not always formed due to 1) the size of the crater (proportional to energy production and presence of high-gradient heat sources) and 2) lithological properties (porosity, availability of water) (Naumov, 2002; Naumov, 2005). The majority of impact-generated hydrothermal systems form in complex craters (>2–4 km) on Earth, however, some do form in simple craters (Osinski et al., 2013). Any hypervelocity impact capable of forming a complex crater will generate a hydrothermal system so long as there is water present (Kirsimäe and Osinski, 2012; Osinski and Pierazzo, 2012).

1.2.1 Heat sources

There are three potential heat sources for hydrothermal systems at impact craters (Osinski et al., 2005; Osinski and Pierazzo, 2012; Osinski et al., 2013):

- (1) Impact melt rocks and melt-bearing breccias;

- (2) Elevated geothermal gradient in the central uplift; and
- (3) Heat in the central uplift due to the passage of shock- and rarefaction waves.

The generation of these heat sources occur during excavation and modification of an impact crater and are dependent on size of the size of the impact and the target rocks. The melt-bearing impactites are the dominant contributor of heat, giving a magnitude of tens to hundreds of times more energy than the elevated geothermal gradient in the central uplift (Daubar and Kring, 2001). However, when shock heating is factored in, the heat contribution from the structural uplift is similar to the heat contribution from the melt-bearing impactites (Thorsos et al., 2001). The duration of thermal output is dependent on the size of the crater. When compared to the impact melt sheet, the thermal output duration from the central uplift is longer in craters $< \sim 130$ km in diameter and shorter in craters $> \sim 130$ km in diameter (Daubar and Kring, 2001). The contribution of heat from central uplifts due to the shock- and rarefaction waves is not yet quantified, although it is assumed to be a very minor heat source (Osinski et al., 2005; Osinski and Pierazzo, 2012; Osinski et al., 2013).

1.2.2 Fluid Sources

H₂O is required as it is the primary fluid circulated in a hydrothermal system (Norton, 1984). Hydrothermal systems have been theorized to be associated with impact events on planetary bodies that are rich in H₂O (Newsom, 1980; Naumov, 2005; Osinski et al., 2013). Due to the abundance of H₂O on Earth, hypervelocity impacts should disrupt the hydrosphere with the exception of small craters and craters formed in arid environments (Osinski et al., 2001; Naumov, 2002; Osinski, 2005; Osinski et al., 2013). Depending on geological setting, seawater and/or meteoric water are the principal sources for hydrothermal fluids at impact craters. Volatiles from the target rocks do contribute, especially early on in sedimentary target lithologies (Kieffer and Simonds, 1980; Naumov, 2005).

1.2.3 Porosity and permeability

An impact-generated hydrothermal system requires an environment favorable for transport. The shocked, fragmented, and displaced nature of impactites at impact craters

result in high porosity and permeability in (allochthonous) impact melt-bearing and lithic breccias, in-situ (autochthonous) target lithologies, and near surface impactites from crater modification (Pilkington and Grieve, 1992). Impact-generated hydrothermal mineralization occurs in porous areas, such as vesicles and fractures, within these units (Naumov, 2005; Osinski, 2005; Osinski et al., 2013).

1.2.4 Alteration Setting

Hydrothermal alteration is characterized by the zonal distribution of alteration minerals and products related to the mass transfer between minerals and the circulating fluids as temperature decreases over the lifespan of the hydrothermal system (Helgeson, 1969; Kirsimäe and Osinski, 2012). Shocked minerals are more soluble and, therefore, more elements are readily available to enter the hydrothermal system. Silicates shocked to from pressures of 7.5 to 22 GPa show a magnitude upwards of 20 times mass-normalized increase of silicon release into a substrate when compared to their non-shocked counterparts (Boslough and Cygan, 1988). Fracture distribution, porosity, permeability, and the distance and energy from heat sources influence the geospatial distribution and morphology of the zones of alteration (Gudmundsson et al., 2002; Meunier, 2003; Kirsimäe and Osinski, 2012). Mineralization can occur at contacts, such as the top and bottom of melt sheets. These contacts act fluid highways, areas where fluids have the path of least resistance to flow (Gudmundsson et al., 2002). It has been proposed that post-impact hydrothermal alteration can occur in six main locations within and proximal to an impact crater (Figure 3) (Osinski et al., 2013):

- (1) Crater fill impact melt rocks and melt-bearing breccias;
- (2) Interior of the central uplift;
- (3) Outer margin of the central uplift;
- (4) Impact ejecta deposits;
- (5) Crater rim; and
- (6) Post-impact crater lake sediments.

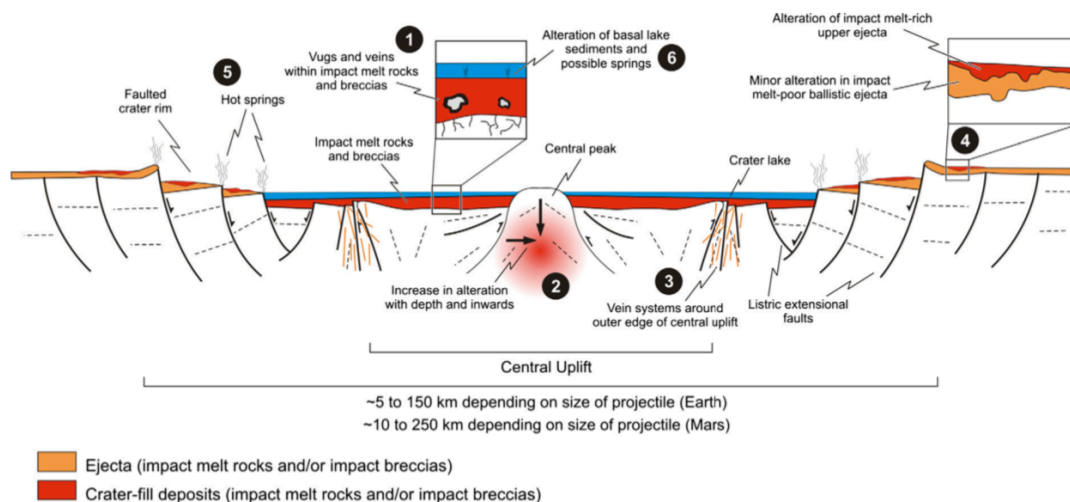


Figure 3: Impact-generated hydrothermal deposits found at typical complex craters.
From Osinski et al., 2013.

1.2.4.1 Crater fill impact melt rocks and melt-bearing breccias

These melt-bearing impactites are themselves a major heat source for potential hydrothermal systems. These systems form zoned alteration phases that change with depth. The system can produce a range of alteration styles from discrete cavity and fracture-filling (e.g., Haughton; see Osinski et al., 2001) to complete and pervasive (e.g., Ries. See Osinski, 2005).

1.2.4.2 Interior of the Central Uplift

Central uplifts comprise of fault-bounded blocks of coherent to brecciated target rock cross-cut by injection dykes of melt-bearing or lithic breccias (Osinski et al., 2013). The main heat source driving alteration in the central uplift is the elevated geothermal gradient (Naumov, 2005). Alteration can be zoned generally restricted to discrete vug and vein filling cavities and fractures (Osinski et al., 2013).

1.2.4.3 Outer margin of the central uplift

These regions are structural ring of highly fractured and faulted, uplifted, sub-vertical-to-overturned strata due to the interaction between the inward-collapsing crater wall and the outward-collapsing edge of the central uplift (Kenkmann and Dalwigk, 2000; Osinski and

Spray, 2005). Alteration is present in the form of fracture-infilling vein networks (Hode et al., 2003; Osinski et al., 2005). It is likely these regions were buried by crater fill impact melt rocks and breccias (Osinski et al., 2005).

1.2.4.4 Impact ejecta deposits

Ejecta is found at relatively fresh impact craters on Earth. Ejecta deposits comprise of two layers (Osinski et al., 2011). The first deposited is ambient temperature deposited lithic breccias. Overlying these breccias are melt-bearing breccias that would have been emplaced at much higher temperatures (e.g., >750–900 °C at Ries) (Osinski et al., 2004). The intensity of alteration varies in ejecta from the same crater, and is affected by the presence of water, such as crater lake (Osinski et al., 2004; Osinski, 2005; Osinski et al., 2013). The heat source of ejecta deposits is entirely from the deposits themselves. Larger craters will contain higher melt volumes, which will result in longer lasting impact ejecta hydrothermal systems (Grieve and Cintala, 1992).

1.2.4.5 Crater rim

Comprised of km-scale, usually listric, extensional faults that along with the surrounding fractured rocks host potential fluid pathways (Osinski et al., 2013). Most craters on Earth do not have well preserved surface exposure of these faults. Haughton has a faulted rim complex dotted with hydrothermal “pipe” structures that are likely hydrothermal vents expressed as hot springs and/or fumaroles (Osinski et al., 2005).

1.2.4.6 Post-impact crater lake sediments

Impact craters can form a sedimentary basin. Impact crater lakes are relatively common on Earth. If the lake formed shortly after impact, sediments of the crater lake would have experienced alteration by the hydrothermal system of the impact crater (Osinski et al., 2013).

1.3 Outro

East and West Clearwater are respectively ~26 km and ≥36 km impact craters located ~125 km east of Hudson’s Bay in northern Quebec at 56°10'N, 74°20'W (Grieve, 2006;

Schmieder et al., 2015; Osinski, 2015). Observations from a drilling program that lasted from 1963–1964 suggested both East and West Clearwater were impact craters (Dence et al., 1965). Previous work has been done on the impact melt sheet (e.g., Palme et al., 1979) and to find the impactor (e.g., Grieve et al., 1981; Evans et al., 1993; Shukolyukov and Lugmair, 2001; McDonald, 2002; Koeberl et al., 2007), and to constrain the age (e.g., Reimold et al., 1981; Bottomley et al., 1990; Schmieder et al., 2015). The impact-generated hydrothermal system has not been a focus until this paper. The intent of this paper is to characterize the secondary mineralogy, zones of alteration, and comparative analysis to other impact-generated hydrothermal system.

Bibliography

- Abramov O. and Kring D. A. (2005) Impact-induced hydrothermal activity on early Mars. *J. Geophys. Res.* **110**.
- Ahrens T. J. and O'Keefe J. D. (1972) Shock melting and vaporization of lunar rocks and minerals. *The Moon* **4**, 214–249.
- Barringer D. M. (1905) Coon Mountain and Its Crater. *Proc. Acad. Nat. Sci. Phila.* **57**, 861–886.
- Bland P. A. and Artemieva N. A. (2003) Efficient disruption of small asteroids by Earth's atmosphere. *Nature* **424**, 288–291.
- Boslough M. B. and Cygan R. T. (1988) Shock-enhanced dissolution of silicate minerals and chemical weathering on planetary surfaces. In *Lunar and Planetary Science Conference Proceedings* pp. 443–453.
- Bottomley R. J., York D. and Grieve R. A. F. (1990) Argon-40-argon-39 dating of impact craters. In *Lunar and Planetary Science Conference Proceedings* pp. 421–431.
- Carr M. H., Baum W. A., Blasius K. R., Briggs G. A., Cutts J. A., Duxbury T. C., Greeley R., Guest J., Masursky H. and Smith B. A. (1980) Viking orbiter views of Mars. *NASA Spec. Publ.* **441**.
- Chao E. C. T., Shoemaker E. M. and Madsen B. M. (1960) First Natural Occurrence of Coesite. *Science* **132**, 220–222.
- Chladni E. F. F. (1794) *Über den Ursprung der von Pallas gefundenen und anderer ihr ähnlicher Eisenmassen, und über einige damit in Verbindung stehende Naturscheinungen.*, Hartknoch.
- Collins G. S., Melosh H. J. and Osinski G. R. (2012) The Impact-Cratering Process. *Elements* **8**, 25–30.
- Croft S. K. (1980) Cratering flow fields-Implications for the excavation and transient expansion stages of crater formation. In *Lunar and Planetary Science Conference Proceedings* **11**, 2347–2378.
- Croft S. K. (1985) The scaling of complex craters. *J. Geophys. Res.* **90**, C828.
- Daubar I. J. and Kring D. A. (2001) Impact-induced hydrothermal systems: Heat sources and lifetimes. In *32nd Lunar and Planetary Science Conference*. 1727.
- Dence M. R. (1968) Shock zoning at Canadian craters: Petrography and structural implications. *Contrib. Dom. Astrophys. Obs. Vic.* **8**.

- Dence M. R. (1965) The extraterrestrial origin of Canadian craters. *Ann. N. Y. Acad. Sci.* **123**, 941–969.
- Dence M. R., Grieve R. A. and Robertson P. B. (1977) Terrestrial impact structures-Principal characteristics and energy considerations. In *Impact and explosion cratering: Planetary and terrestrial implications*. 247–275.
- Dence M. R., Innes M. J. S. and Beals C. S. (1965) On the probable meteorite origin of the Clearwater Lakes, Quebec. *J. R. Astron. Soc. Can.* **59**, 13–22.
- Durack P. J., Wijffels S. E. and Matear R. J. (2012) Ocean Salinities Reveal Strong Global Water Cycle Intensification During 1950 to 2000. *Science* **336**, 455–458.
- Evans N. J., Gregoire D. C., Grieve R. A. F., Goodfellow W. D. and Veizer J. (1993) Use of platinum-group elements for impactor identification: Terrestrial impact craters and Cretaceous-Tertiary boundary. *Geochim. Cosmochim. Acta* **57**, 3737–3748.
- French B. M. (1998) Traces of Catastrophe: A Handbook of Shock-Metamorphic Effects in Terrestrial Meteorite Impact Structures. *Lunar and Planetary Institute* **954**.
- French B. M. and Short N. M. (1968) Shock metamorphism of natural materials: proceedings. *Mono Book Corp.*
- Galilei G. (1610) Sidereus Nuncius. *Thomas Baglionus* **58**.
- Gault D. E., Quaide W. L. and Oberbeck V. R. (1974) Impact cratering mechanics and structures. In *A Primer in Lunar Geology*, 177–189.
- Gault D. E., Quaide W. L. and Oberbeck V. R. (1968) Impact cratering mechanics and structures. In *Shock Metamorphism of Natural Materials*. *Mono Books Corp*, 87–99.
- Gilbert G. K. (1893) The Moon's Face: A Study of the Origin of Its Features. *Philosophical Society of Washington*.
- Grieve R. A. and Cintala M. J. (1981) A method for estimating the initial impact conditions of terrestrial cratering events, exemplified by its application to Brent crater, Ontario. In *12th Lunar and Planetary Science Conference Proceedings*, 1607–1621.
- Grieve R. A., Dence M. R. and Robertson P. B. (1977) Cratering processes-As interpreted from the occurrence of impact melts. In *Impact and Explosion Cratering: Planetary and Terrestrial Implications*, 791–814.
- Grieve R. A. F. (2006) Impact Structures in Canada. *Geological Association of Canada*.
- Grieve R. A. F. (1991) Terrestrial impact: The record in the rocks. *Meteoritics* **26**, 175–194.

- Grieve R. A. F. and Cintala M. J. (1992) An analysis of differential impact melt-crater scaling and implications for the terrestrial impact record. *Meteoritics* **27**, 526–538.
- Grieve R. A. F., Palme H. and Plant A. G. (1981) Siderophile-rich particles in the melt rocks at the E. Clearwater impact structure, Quebec: Their characteristics and relationship to the impacting body. *Contrib. Mineral. Petrol.* **75**, 187–198.
- Grieve R. A. F. and Robertson P. B. (1979) The terrestrial cratering record: I. Current status of observations. *Icarus* **38**, 212–229.
- Grieve R. A. F. and Therriault A. M. (2004) Observations at terrestrial impact structures: Their utility in constraining crater formation. *Meteorit. Planet. Sci.* **39**, 199–216.
- Gudmundsson A., Fjeldskaar I. and Brenner S. L. (2002) Propagation pathways and fluid transport of hydrofractures in jointed and layered rocks in geothermal fields. *J. Volcanol. Geotherm. Res.* **116**, 257–278.
- Helgeson H. C. (1969) Thermodynamics of hydrothermal systems at elevated temperatures and pressures. *Am. J. Sci.* **267**, 729–804.
- Hergarten S. and Kenkmann T. (2015) The number of impact craters on Earth: Any room for further discoveries? *Earth Planet. Sci. Lett.* **425**, 187–192.
- Hode T., von Dalwigk I. and Broman C. (2003) A hydrothermal system associated with the Siljan Impact Structure, Sweden—Implications for the search for fossil life on Mars. *Astrobiology* **3**, 271–289.
- Impact Earth (2018) Impact Crater Database. <https://impact.uwo.ca/map/> [Accessed December 19, 2018].
- Ivanov B. A. (2004) Heating of the lithosphere during meteorite cratering. *Sol. Syst. Res.* **38**, 266–279.
- Ivanov B. A., Bazilevskiy A. T. and Sazonova L. V. (1982) Formation of the central uplift in meteoric craters (in Russian; English technical translation 1986, NASA TM-88427). *Метеоритика* **40**, 60–81.
- Johnson B. C. and Bowling T. J. (2014) Where have all the craters gone? Earth's bombardment history and the expected terrestrial cratering record. *Geology* **42**, 587–590.
- Kenkmann T. and Dalwigk I. von (2000) Radial transpression ridges: A new structural feature of complex impact craters. *Meteorit. Planet. Sci.* **35**, 1189–1201.
- Kieffer S. W. and Simonds C. H. (1980) The role of volatiles and lithology in the impact cratering process. *Rev. Geophys.* **18**, 143–181.

- Kirsimäe K. and Osinski G. R. (2012) Impact-Induced Hydrothermal Activity. In *Impact Cratering*. Wiley-Blackwell, 76–89.
- Koeberl C., Shukolyukov A. and Lugmair G. W. (2007) Chromium isotopic studies of terrestrial impact craters: Identification of meteoritic components at Bosumtwi, Clearwater East, Lappajärvi, and Rochechouart. *Earth Planet. Sci. Lett.* **256**, 534–546.
- Kominz M. A. (2001) Sea Level Variations Over Geologic Time. In *Encyclopedia of Ocean Sciences*. Elsevier, 2605–2613.
- Maxwell D. E. (1977) Simple Z model of cratering, ejection, and the overturned flap. In *Impact and Explosion Cratering*. Pergamon, 1003–1008.
- McDonald I. (2002) Clearwater East impact structure: A re-interpretation of the projectile type using new platinum-group element data from meteorites. *Meteorit. Planet. Sci.* **37**, 459–464.
- Melosh H. J. (1989) Impact Cratering: A Geologic Process. *Oxf. Univ. Press*.
- Melosh H. J. (1985) Impact cratering mechanics: Relationship between the shock wave and excavation flow. *Icarus* **62**, 339–343.
- Melosh H. J. and Ivanov B. A. (1999) Impact crater collapse. *Annu. Rev. Earth Planet. Sci.* **27**, 385–415.
- Meunier A. (2003) Clays). *Editions Scientifiques GB (Fr); Springer Science & Business Media (En)*.
- National Research Council (US) (1979) Continental margins: Geological and geophysical research needs and problems. *National Academies Press*.
- Naumov M. V. (2002) Impact-generated hydrothermal systems: Data from Popigai, Kara, and Puchezh-Katunki impact structures. In *Impacts in Precambrian shields*. Springer, 117–171.
- Naumov M. V. (2005) Principal features of impact-generated hydrothermal circulation systems: mineralogical and geochemical evidence. *Geofluids* **5**, 165–184.
- Newsom H. E. (1980) Hydrothermal alteration of impact melt sheets with implications for Mars. *Icarus* **44**, 207–216.
- Norton D. L. (1984) Theory of hydrothermal systems. *Annu. Rev. Earth Planet. Sci.* **12**, 155–177.
- O’Keefe J. D. and Ahrens T. J. (1982) Cometary and meteorite swarm impact on planetary surfaces. *J. Geophys. Res. Solid Earth* **87**, 6668–6680.

- Osinski G. R. (2005) Hydrothermal activity associated with the Ries impact event, Germany. *Geofluids* **5**, 202–220.
- Osinski G. R. (2015) Revisiting the West Clearwater Lake Impact Structure, Canada. In *46th Lunar and Planetary Science Conference*, 1621.
- Osinski G. R., Grieve R. A. F., Bleacher J. E., Neish C. D., Pilles E. A. and Tornabene L. L. (2018) Igneous rocks formed by hypervelocity impact. *J. Volcanol. Geotherm. Res.* **353**, 25–54.
- Osinski G. R., Grieve R. A. F. and Spray J. G. (2004) The nature of the groundmass of surficial suevite from the Ries impact structure, Germany, and constraints on its origin. *Meteorit. Planet. Sci.* **39**, 1655–1683.
- Osinski G. R., Lee P., Parnell J., Spray J. G. and Baron M. (2005) A case study of impact-induced hydrothermal activity: The Haughton impact structure, Devon Island, Canadian High Arctic. *Meteorit. Planet. Sci.* **40**, 1859–1877.
- Osinski G. R. and Pierazzo E. (2012) Impact cratering: Processes and products. In *Impact cratering: Processes and products*. Wiley-Blackwell, 1–20.
- Osinski G. R. and Spray J. G. (2005) Tectonics of complex crater formation as revealed by the Haughton impact structure, Devon Island, Canadian High Arctic. *Meteorit. Planet. Sci.* **40**, 1813–1834.
- Osinski G. R., Spray J. G. and Lee P. (2001) Impact-induced hydrothermal activity within the Haughton impact structure, arctic Canada: Generation of a transient, warm, wet oasis. *Meteorit. Planet. Sci.* **36**, 731–745.
- Osinski G. R., Tornabene L. L., Banerjee N. R., Cockell C. S., Flemming R., Izawa M. R. M., McCutcheon J., Parnell J., Preston L. J., Pickersgill A. E., Pontefract A., Sapers H. M. and Southam G. (2013) Impact-generated hydrothermal systems on Earth and Mars. *Icarus* **224**, 347–363.
- Osinski G. R., Tornabene L. L. and Grieve R. A. F. (2011) Impact ejecta emplacement on terrestrial planets. *Earth Planet. Sci. Lett.* **310**, 167–181.
- Palme H., Göbel E. and Grieve R. A. F. (1979) The distribution of volatile and siderophile elements in the impact melt of East Clearwater Quebec. In *10th Lunar and Planetary Science Conference Proceedings*, 2465–2492.
- Passey Q. R. and Melosh H. J. (1980) Effects of atmospheric breakup on crater field formation. *Icarus* **42**, 211–233.
- Pilkington M. and Grieve R. A. F. (1992) The geophysical signature of terrestrial impact craters. *Rev. Geophys.* **30**, 161.

- Pirajno F. (2009) Hydrothermal Processes Associated with Meteorite Impacts. In *Hydrothermal Processes and Mineral Systems*. Springer, Dordrecht, 1097–1130.
- Quaide W. L., Gault D. E. and Schmidt R. A. (1965) Gravitative effects on lunar impact structures. *Ann. N. Y. Acad. Sci.* **123**, 563–572.
- Reimold W. U., Grieve R. A. F. and Palme H. (1981) Rb-Sr dating of the impact melt from East Clearwater, Quebec. *Contrib. Mineral. Petrol.* **76**, 73–76.
- Robbins S. J. and Hynes B. M. (2012) A new global database of Mars impact craters ≥ 1 km: 1. Database creation, properties, and parameters. *J. Geophys. Res. Planets* **117**.
- Sapers H. M., Osinski G. R., Flemming R. L., Buitenhuis E., Banerjee N. R., Tornabene L. L., Blain S. and Hainge J. (2016) Evidence for a spatially extensive hydrothermal system at the Ries impact structure, Germany. *Meteorit. Planet. Sci.* **52**, 351–371.
- Schmieder M., Schwarz W. H., Trieloff M., Tohver E., Buchner E., Hopp J. and Osinski G. R. (2015) New $^{40}\text{Ar}/^{39}\text{Ar}$ dating of the Clearwater Lake impact structures (Québec, Canada)–Not the binary asteroid impact it seems? *Geochim. Cosmochim. Acta* **148**, 304–324.
- Shoemaker E. M. (1959) Impact mechanics at Meteor Crater, Arizona., *U.S. Geological Survey*.
- Shoemaker E. M. (1960) Penetration Mechanics of High Velocity Meteorites: Illustrated by Meteor Crater, Arizona. *Berlingske bogtr.*
- Shoemaker E. M. (1977) Penetration mechanics of high velocity meteorites, illustrated by Meteor Crater, Arizona. *Meteor. Craters Benchmark Pap. Geol.* **36**, 170.
- Shukolyukov A. and Lugmair G. W. (2001) Extraterrestrial matter on Earth: Evidence from the Cr isotopes. In *Catastrophic Events and Mass Extinctions: Impacts and Beyond*. Geological Society of America, **356**, 3041.
- Stöffler D., Gault D. E., Wedekind J. and Polkowski G. (1975) Experimental hypervelocity impact into quartz sand: Distribution and shock metamorphism of ejecta. *J. Geophys. Res.* **80**, 4062–4077.
- Thorsos I. E., Newsom H. E. and Davies A. G. (2001) Availability of heat to drive hydrothermal systems in large Martian impact craters. In *32nd Lunar and Planetary Science Conference*.

Chapter 2

2 Impact-generated hydrothermal system at East Clearwater

2.1 Introduction

A hydrothermal system is the redistribution of mass and energy through thermal, chemical, and mechanical processes caused by circulating H₂O fluids and molecular diffusion (Norton, 1984). Many impacts on Earth are associated with hydrothermal alteration (Osinski et al., 2013). Evidence of past hydrothermal systems are from the alteration mineralization produced. This study is the first dedicated to the characterization of the hydrothermal alteration at the East Clearwater impact structure.

2.2 Wiyâshâkimî (Clearwater Lake) Complex

Clearwater Lake, lac Wiyâshâkimî in Cree, Lac à l'Eau Claire in French, or Allait Qasigialingat (Cree Lake where there are fresh water seals) in Inuit (Commission de toponymie, 2016), is situated in the Tursujuq Provincial Park in Northern Quebec ~125 km east of Hudson's Bay at 56°10'N, 74°20'W (Figure 4). The two impact crater lakes, the ≥36 km West Clearwater (56°13'N, 74°30'W) and ~26 km East Clearwater (56°05'N, 74°07'W) impact craters are have apparent diameters of 36 km and 26 km, respectively (Grieve, 2006; Schmieder et al., 2015; Osinski, 2015).

In 1956, it was suggested that the Clearwater lakes were of an impact origin (Beals et al., 1956). Material from Clearwater lake drill core was recovered in 1963 and 1964. The presence of allochthonous breccias and recrystallized fragments in a heavily vesiculated crystalline matrix was indicative of an impact origin (Dence, 1964; Dence et al., 1965). Simultaneously, it was proposed that East and West Clearwater were an impact doublet formed from a binary asteroid (Dence et al., 1963; Dence et al., 1965).



Figure 4: Landsat image of the Clearwater Lakes. Modified from (Landsat 8, 2013).

While both East and West Clearwater have similar target lithologies, East Clearwater has geochemical evidence of an impactor, while West Clearwater does not (Palme et al., 1978; Grieve et al., 1981). Initial PGE values indicated the impactor of East Clearwater to be a carbonaceous chondrite (Palme et al., 1978; Grieve et al., 1981), although further PGE work involving Cr indicated it could be an ordinary chondrite (Palme et al., 1979; Evans et al., 1993). However, observed $^{53}\text{Cr}/^{52}\text{Cr}$ ratios are high, which are indicative of ordinary chondrites, as carbonaceous chondrites have low $^{53}\text{Cr}/^{52}\text{Cr}$ ratios (Shukolyukov and Lugmair, 2001; Koeberl et al., 2007). Chromium isotope and more recent PGE ratio analysis indicates it is an ordinary chondrite, and either L- (Evans et al., 1993; McDonald, 2002; Koeberl et al., 2007) or H- (Shukolyukov and Lugmair, 2001; Koeberl et al., 2007) chondrite.

The age of East Clearwater was determined through mineral isochron Rb-Sr dating to be 287 ± 26 Ma (Reimold et al., 1981). The use of ^{40}Ar - ^{39}Ar dating indicated the maximum age of the East Clearwater impact was ≤ 460 Ma (Bottomley et al., 1990). Further ^{40}Ar - ^{39}Ar dating of the East Clearwater impact melt sheet samples indicate West Clearwater impacted in the Permian (286.2 ± 2.2 Ma) and East Clearwater impacted in the Ordovician (~ 460 – 470 Ma) (Schmieder et al., 2015).

Both West and East Clearwater, at only ~ 30 km from centre to centre, impacted into similar target lithologies in the Canadian Shield (Figure 5). Geologically, West and East Clearwater impacted into the northern section of the Bienville Domain, Minto Subprovince, Superior Province (Simard et al., 2008). The Superior Province is an expansive Archean craton that forms the core of the Canadian Shield (Gill, 1949; Wilson, 1949). The Minto Subprovince is a composite volcano-plutonic terrain (Leclair et al., 2006; Simard et al., 2008). The majority of the rocks in the Bienville Domain are of plutonic origin (Simard et al., 2008). Two different lithologies dominate the target rocks of the Clearwater impacts (Figure 5): 1) The Loups Marins Suite (Alma1 & Alma2) (Gosselin and Simard, 2001; Simard et al., 2008); and 2) The Desbergères Suite (Adeb) (Simard et al., 2001; Simard et al., 2008).

Minor components such as the Châteauguay Suite (Achg) are found near the rim of East Clearwater and are certainly part of the target rocks. Other minor units, such as the Qullinaaraaluk Suite (Aluk) (Almost certainly apart of West Clearwater), the Tramont Suite (Atra), the Lesdiguières/Favard Suite (Alsd/ Afav), the Coursolles Suite (Acou), the Sem suite (Asem), and the Maurel Suite (Amau) may have part of the target, but not are found at the rim of the East Clearwater impact crater (See (Simard et al., 2008) for descriptions). The unit descriptions below are translated from (Simard et al., 2008) and related publications.

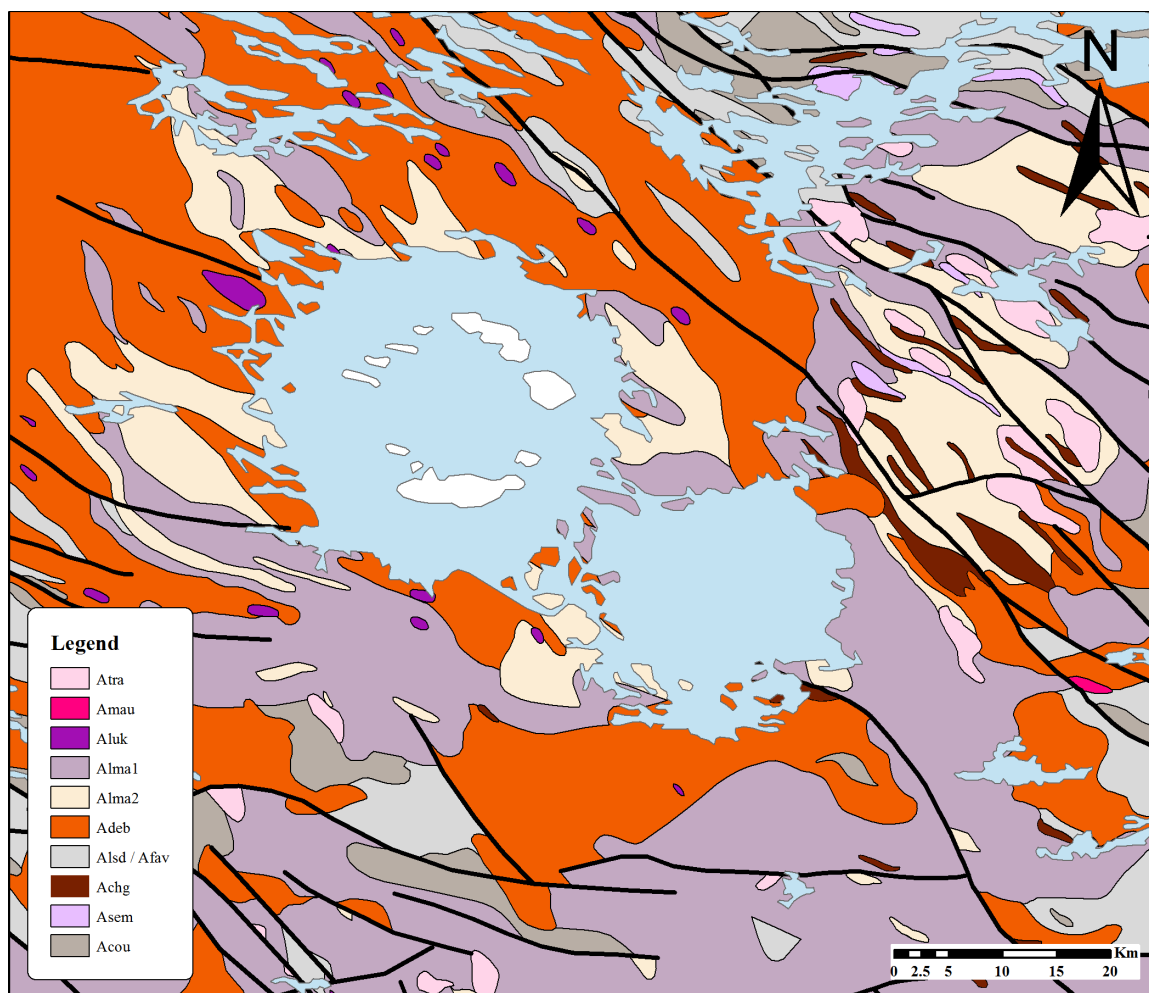


Figure 5. The Geology of the East Clearwater crater complex. From youngest to oldest: Tramont Suite (Atra), Maurel Suite (Amau), Qullinaaraaluk Suite (Aluk), Loups Marins Suite (Cpx-bearing is Alma1; Opx-bearing is Alma2), Desbergères Suite (Adeb), Lesdiguières/Favard Suite (Alsd/Afav), Châteauguay Suite (Achg), Sem suite (Asem), and Coursolles Suite (Acou). Modified from (Simard et al., 2008).

2.2.1 Loups Marins Suite (Alma1 & Alma2)

These highly magnetic rocks show a variable heterogeneity due to partially assimilated enclaves of amphibolite, diorite, and paragneiss, and the variation in granitic material in the rocks. The Loups Marins Suite comprises intrusive pyroxene-bearing felsic rocks that are divided into a clinopyroxene-bearing unit and an orthopyroxene-bearing unit (Gosselin and Simard, 2001).

The clinopyroxene-bearing unit (Alma1) comprises equigranular to porphyritic rocks that are medium to coarse grained, massive to slightly foliated, with a purplish hue. The lithologies of the clinopyroxene-bearing unit include tonalite, quartz diorite, granodiorite, and granite. Burgundy plagioclase is responsible for the purplish hue. The age of the clinopyroxene-bearing unit is 2715 to 2705 Ma, although ages in the range of the orthopyroxene-bearing rocks have been found (Gosselin and Simard, 2001; Simard et al., 2008).

The orthopyroxene-bearing unit (Alma2) comprises rocks that are medium to coarse grained, massive to foliated, with a green-brown colouration. The lithologies of the orthopyroxene-bearing unit includes enderbite and hypersthene bearing quartz diorite, with small amounts of opdalite and charnockite. Kilometer-sized lenses are present, composed of gabbro, hypersthene diorite, and a small amount of ultramafic rocks. The age of the orthopyroxene-bearing unit is 2735 and 2720 Ma, although younger dates have been found in this unit (Simard et al., 2008).

2.2.2 Desbergères Suite (Adeb)

The Desbergères Suite is composed of homogenous granodiorite and granite that are medium to coarse grained, massive to slightly foliated, with a grey or pink colouration. These rocks contain 1–8% biotite in granite and both biotite and hornblende in granodiorite. Generally, 5% is 5 cm potassic feldspar phenocrysts, although localities can be greater than 25%. Kilometre-scale porphyritic intrusions can contain 15–35% potassic feldspar. Tonalite enclaves are present near diffuse contacts (Simard et al., 2001; Simard et al., 2008; Simard, 2008). The rocks are dated to 2720–2710 Ma (Simard et al., 2008).

2.2.3 Châteauguay Suite (Achg)

This unit comprises granoblastic, intermediate to ultramafic, massive to foliated dykes and sills. They contain injected white felsic material that gives the rocks a brecciated appearance. The dykes and sills are a few meters thick by kilometers long. Intermediate rocks include diorite and rarely quartz diorite. Mafic rocks are dominated by gabbro and gabbro. Ultramafic rocks include peridot, pyroxenites, and hornblende. No date

has been measured, but observations indicate between 2740 and 2710 Ma (Simard et al., 2001; Simard et al., 2008).

2.2.4 Impactites

Material from East Clearwater was recovered during a drilling program in 1963 and 1964 (Dence, 1964; Dence et al., 1965). Drilling occurred in the winter on the frozen lake, penetrating through 87 m of water, 46 m of unconsolidated glacial debris including boulders, and glacial sediments consisting of interbedded limestone, shale, and gritty sandstone until a core depth of 245 m (233 m in actual depth) (Dence et al., 1963; Dence et al., 1965). As drilling proceeded, the drill angle continued to deviate from the normal. Once the drill had reached the impact melt sheet, it was off by 30°. As a result, most of the core above the melt sheet was not recovered, and only the top 46 m of the impact melt-bearing breccias and melt sheet were extracted before drilling had to be terminated (Palme et al., 1979). The impact melt sheet at East Clearwater has been described in past studies (Dence et al., 1965; Palme et al., 1979). This study agrees with the past descriptions, except for the top of the melt sheet. The impactites can be divided into three petrographic units:

- 1) Breccia unit: Dark green inclusion-rich fine-grained impact melt-bearing breccia (~4.5m thick);
- 2) Vesicular impact melt rock: Light grey vesicular impact melt rock (~7.5m thick);
- 3) fine-grained coherent impact melt rock: Dark green fine-medium (increasing with depth) grained impact melt rock (~34m thick)



Figure 6: A. Upper Zone 1. section from the impact melt-bearing breccia at 271.6 m (sample 948.5). B. Lower Zone 1. Vesicular impact melt rock. 279.4 m (sample 2-63-978). C. Zone 2. Fine-grained coherent impact melt rock. 308.7 m (sample 1089).

2.2.5 Previous Noted Alteration

Impact-induced hydrothermal alteration has been observed throughout the melt sheet of East Clearwater, but only in passing. Chloritization of the melt sheet was noticed in (Dence, 1965). Accounts from Grieve et al. (1981) noted there were secondary mineralization in the form of millerite, galena, and sphalerite. Palme et al. (1979) noted the presence of clay minerals, quartz, calcite, fluorite, chalcopryrite, sphalerite, and millerite, and interpreted the sulfides to have formed from a sulfur-rich vapour phase that rose to the top during conductive cooling.

2.3 Methods

2.3.1 Samples

All of the samples in this study come from one drill core (2-63) from East Clearwater. Of the two cores drilled at East Clearwater, this is the only drill core that sampled the impact

melt sheet. From 37 pieces of East Clearwater 2-63 core, 38 thin sections were produced. All thin sections were cut, polished, and mounted in the absence of water to preserve hydrologically sensitive and potentially friable minerals including zeolites, chlorites, and clays. All samples cut for this study are from the impact-bearing breccias and impact melt sheet. Some samples from West Clearwater were briefly observed for comparison purposes. Most agreed with descriptions in previous work (e.g., Phinney et al., 1978), and a centimetre-scale wide hematite vein was found.

2.3.2 Analytical methods

Samples were investigated using a combination of optical petrography, Electron Micro-Probe Analysis (EMPA), in-situ X-ray Diffraction (XRD), Raman spectroscopy, and UV-Vis-NIR spectroscopy via Analytical Spectral Device (ASD) on thin sections and drill cores to characterize the secondary mineral assemblages. Veins and vugs were the primary targets, as these features are related to the hydrothermal system and contain alteration minerals.

The Electron MicroProbe Analyzer (EMPA) used was a JEOL JXA-8530F Field Emission Electron Probe Microanalyzer. It is able to detect elements from B to U. Samples were carbon coated. Qualitative assessments were made using Energy Dispersive X-ray Spectroscopy (EDS) techniques, and quantitative measurements by Wavelength Dispersive X-ray Spectroscopy (WDS). Qualitative element maps were produced from both EDS and WDS.

General hydrous silicate standards (20 nA probe current at 15 kV; 5 μm beam diameter): albite (Si, Al, Na); anorthite (Ca); fayalite (Fe); diopside (Mg); orthoclase (K); pollucite (Cs, Rb); barite (Ba); celestite (Sr); and apatite (P).

Zeolite standards (20 nA probe current at 20 kV; 5 μm beam diameter): albite (Si, Al, Na); diopside (Ca, Mg); fayalite (Fe); orthoclase (K); pollucite (Cs); RbTiOPO_4 (Rb); barite (Ba); celestite (Sr); and apatite (P).

Sulfide standards (60 nA probe current at 20 kV; 1 μm beam diameter): sphalerite (Zn, S); pyrite (Fe, S); galena (Pb, S); millerite (Ni); chalcopyrite (Cu, Fe); tin (Sn); silver (Ag); cadmium (Cd); and indium (In).

In-situ micro X-ray diffraction (μXRD) analysis was completed using a Bruker AXS D8 Discover microdiffractometer. μXRD used Cu $K\alpha$ radiation ($\lambda = 1.5418 \text{ \AA}$), producing a 500 μm diameter beam on a triple axis mobile stage. Raman spectroscopy was gathered using a Renishaw InVia Reflex Raman Spectrometer with three available wavelengths (785nm, 633nm, 514nm). The ASD spectrometer used is a Malvern Panalytical ASD FieldSpec 4 Hi-Res: High Resolution Spectroradiometer. It has a 3 nm VNIR (700 nm) and an 8 nm SWIR (1400/2100 nm) spectral resolution. A full range solar irradiance spectral range (350–2500 nm) with spectral sampling (bandwidth) of 1.4 nm for 350–1000 nm and 1.1 nm for 1001–2500 nm.

2.4 Results

Based on optical petrography and EMPA analyses, 2 hydrothermal zones have been defined, characterized by distinct types of hydrothermal alteration (Figure 17). Zone 1 is defined by the zeolite and clay assemblages. Zone 2 is defined by chlorite and to a lesser extent, radial quartz assemblages. The petrographic division between the vesiculated melt and the non-vesiculated melt line up closely with hydrothermal alteration styles, however, multiple altered glass spherules that occasionally contain orthoclase at the centre surrounded by chlorite exist at the topmost of the impact melt-bearing breccia unit (Figure 17).

2.4.1 Zone 1

Zone 1 is characterized by centimetre- to decimetre- wide vugs filled with nickel-rich sulfides (i.e., millerite, vaesite-pyrite) and zeolites (i.e., clinoptilolite-Ca, heulandite-Ca). Pb-Zn-Cu-Fe sulfides (i.e., galena, sphalerite, chalcopyrite, pyrite), quartz, calcite and smectites (i.e., saponite) and other clays are also present in lesser amounts. Upper Zone 1 (Figure 6) contains vugs that are 75-100% filled with zeolites, sulfides, quartz, and clays. These vugs are filled with visible red and white material (Figure 6A). The white material

is mostly zeolites with minor quartz, and the red colour is caused by the oxidation haloes surrounding nickel rich sulfides of vaesite-pyrite and millerite that is encased in a radial heulandite. All occurrences of these sulfides in Zone 1 are always encased by zeolites. Lower Zone 1 (Figure 6B) contains largely empty vugs that can be filled 0–10% by millerite, and by <5% zeolites. No oxidation is visible, and millerite exists as centimetre long needles that are not encased. In the impact melt-bearing breccias, chlorite is present in altered glass beads occasionally surrounding orthoclase, and as a pervasive chloritization is present in the silicate melt of the first, giving the matrix a dark green colour (Figure 6).

2.4.1.1 Sulfides

Two groups of sulfides are observed in the vugs at the top of the melt sheet of East Clearwater. The first group consists of the nickel-rich sulfides of millerite and vaesite-pyrite. The second group contains galena, sphalerite, pyrite, and chalcopyrite.

2.4.1.1.1 Nickel-iron Sulfides

This sulfide group consists of the nickel-rich sulfides of millerite $[\text{Ni}_{(0.95-0.98)}\text{Fe}_{(0.02-0.05)}\text{S}_{(0.99-1.01)}]$ (Figure 7; Table 1) and a solid solution on the vaesite-pyrite scale $[\text{Ni}_{(0.49-0.66)}\text{Fe}_{(0.34-0.51)}\text{S}_{(2.00-2.01)}]$ (Figure 7; Table 1). Most vugs in lower Zone 1 only contain these sulfides and no other, or very minor zeolite mineralization. Millerite occurs throughout Zone 1 and is acicular and radial from nucleation points along the walls of vugs. Lower Zone 1, millerite crystals are prominent enough that they can be seen with the naked eye in many vugs. In upper Zone 1, millerite is relatively intact and does not seem to have been greatly affected by the growth of radial clinoptilolite-Ca (Figure 7; Figure 8). Vaesite-pyrite is not observed as frequently, but when present it is associated with millerite. Vaesite-pyrite is found as octahedral crystals at nucleation points that millerite radiates from and is slightly to almost completely oxidized (Figure 7). A red oxidation halo of hematite (Figure 8) is almost always associated with both these nickel-rich sulfides, although sometimes no sulfides are seen at their centres. The oxidation halos are a few millimetres wide and are observed in most of the thin sections in upper

Zone 1 (Figure 8). These oxidation haloes are iron-rich spheres of hematite that are encased within radial clinoptilolite-Ca.

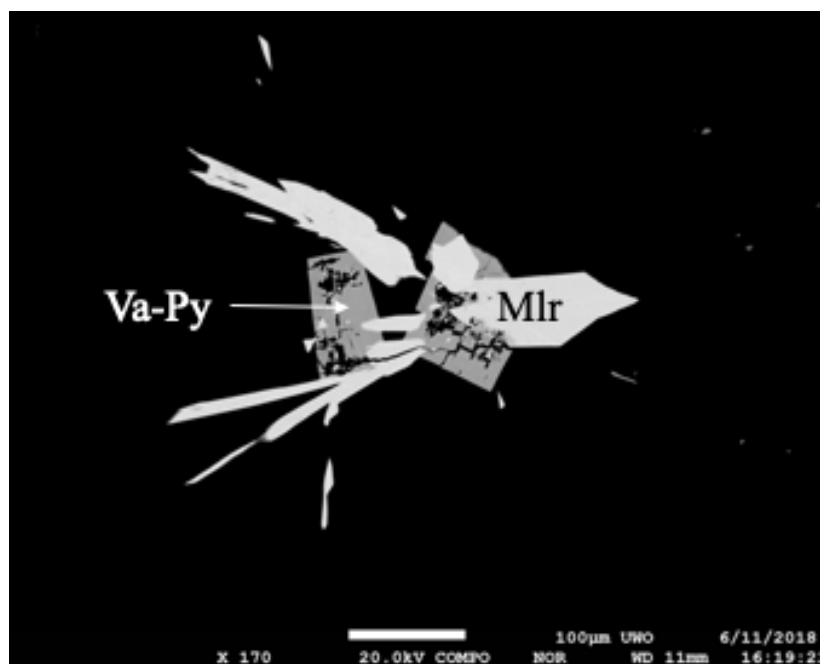


Figure 7: Millerite (Mlr) and vaesite-pyrite (Va-Py). Millerite is acicular and radiates out from a point. Vaesite-pyrite is octahedral and moderately altered.

Table 1: Ni-Fe Sulfide WDS. Millerite and Vaesite-pyrite. b.d. indicates “below detection”.

Mass%	Millerite		Vaesite-pyrite		
	1	2	3	4	5
S	35.645	35.745	53.384	53.794	53.539
Ni	62.622	64.062	32.176	23.791	30.055
Fe	3.323	1.561	15.902	23.837	17.668
Pb	0.082	0.175	0.129	0.175	0.168
Co	b.d.	b.d.	0.016	0.036	0.039
Ag	b.d.	0.01	0.014	0.007	b.d.
Cu	b.d.	b.d.	b.d.	0.027	b.d.
Cd	b.d.	0	b.d.	b.d.	0
In	b.d.	0.001	b.d.	b.d.	b.d.
Zn	b.d.	b.d.	b.d.	b.d.	0.001
Sn	b.d.	b.d.	b.d.	b.d.	b.d.
Total	101.672	101.554	101.621	101.667	101.47

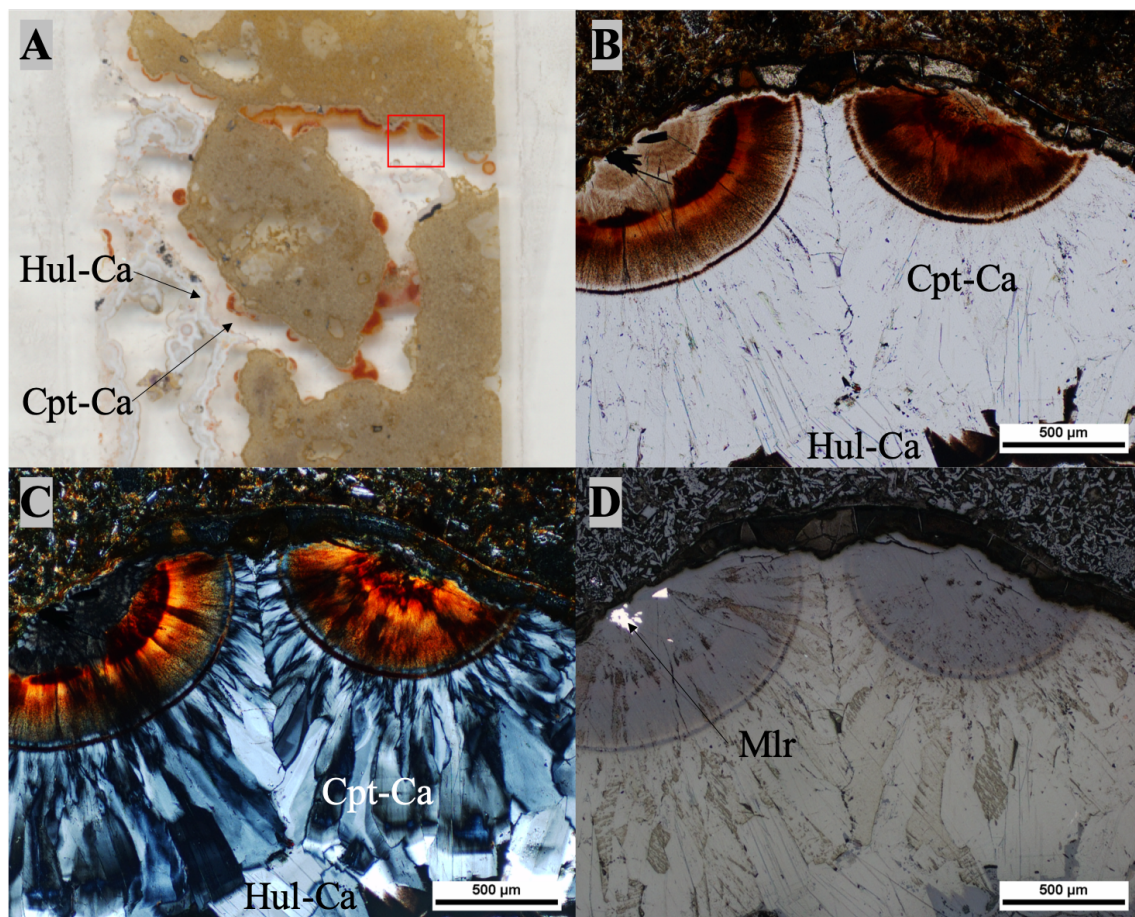


Figure 8: Red Oxidation Halo emanating from millerite (Mlr) and vaesite-pyrite at 271.2 m depth. A. Oxidation halos visible from the top of the melt sheet. The red box indicates the location of images B-D in this figure B. PPL image of the alteration haloes. They are inside clinoptilolite-Ca (Cpt-Ca) crystals. C. XPL image showing the tabular nature of the clinoptilolite-Ca. Two points of nucleation are present. D. BSE reveals the millerite at the centre of the alteration halo on the left. There appears to be none in the one on the right.

2.4.1.1.2 Pb-Zn-Cu-Fe Sulfides

The Pb-Zn-Cu-Fe group of sulfides consist of galena [$\text{Pb}_{(0.98)}\text{Zn}_{(0.01-0.02)}\text{Cu}_{(0.00-0.01)}\text{S}_{(0.99-1.00)}$], sphalerite [$\text{Zn}_{(0.99-1.00)}\text{Fe}_{(0.00-0.01)}\text{Cd}_{(0.00-0.01)}\text{S}_{(1.00)}$], chalcopyrite [$\text{Cu}_{(0.50)}\text{Fe}_{(0.49)}\text{S}_{(0.98)}$] or [$\text{Cu}_{(1.01)}\text{Fe}_{(0.99)}\text{S}_{(1.96)}$], and pyrite (Figure 9,

Table 2). These sulfides are all found in upper Zone 1 and are usually at the edge of radial clinoptilolite-Ca or within the botryoidal heulandite-Ca (Figure 9). Galena and sphalerite are also commonly found in lower Zone 1.

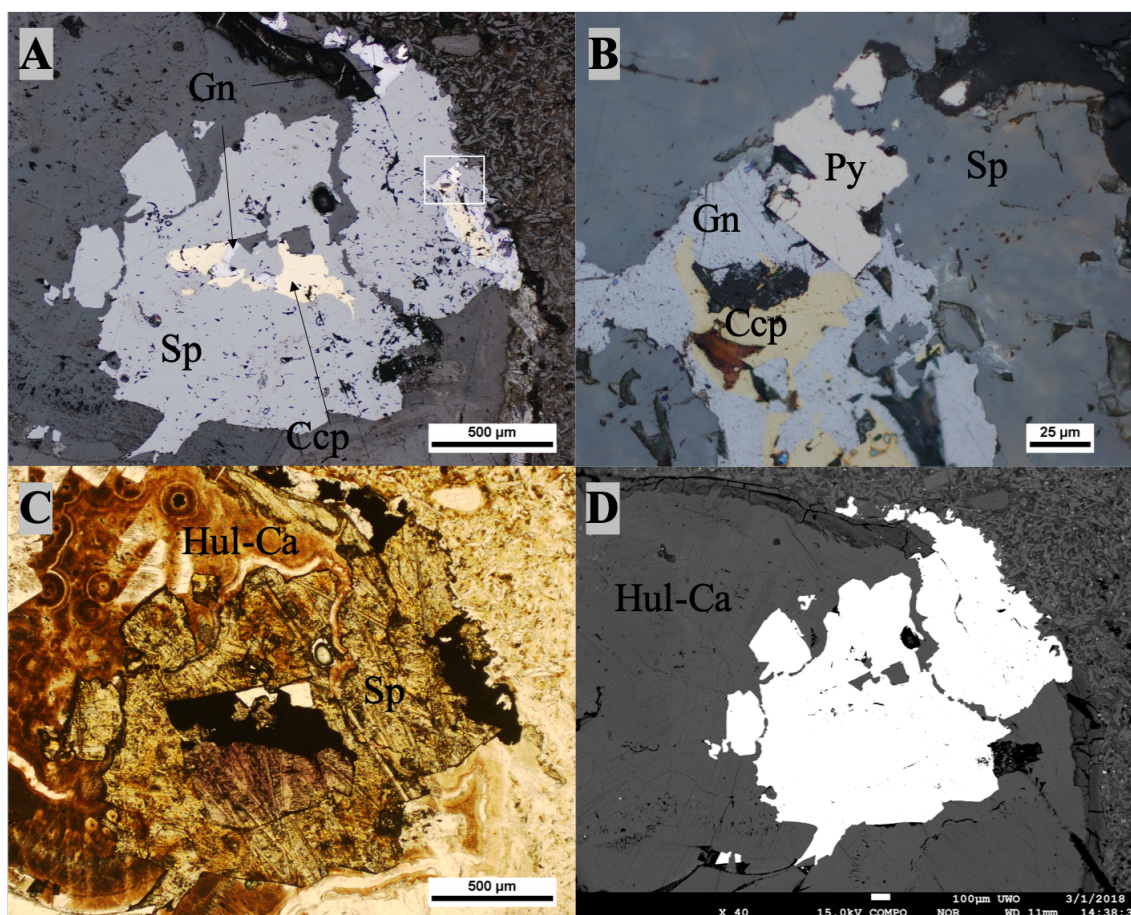


Figure 9: The Pb-Zn-Cu-Fe group of sulfides found at East Clearwater at 271.2 m depth. A. Reflected light image of a large sphalerite (Sp) with other sulfides encased in it. The white box indicates the location of B in this figure. B. A section of A showing all four sphalerite, galena (Gn), chalcopyrite (Ccp), and pyrite (Py). C&D.

Plane polarized light and back scattered electron image showing the botryoidal heulandite-Ca (Hul-Ca), respectively.

Table 2: Geochemistry of the Pb-Zn-Cu-Fe sulfides. b.d. indicates “below detection”.

Mass%	Sphalerite				Chalcopyrite		Galena	
	1	2	3	4	5	6	7	8
S	33.005	33.022	32.465	33.06	34.874	34.864	13.762	13.626
Zn	66.902	67	65.871	66.689	0.048	0.107	0.432	0.208
Fe	0.121	0.083	0.029	0.329	30.569	30.579	0.039	0.069
Cu	0.059	0.071	0.03	0.249	35.497	35.48	0.095	0.158
Pb	0.124	0.097	0.06	0.071	0.118	0.104	86.648	86.958
Ni	0.001	0.002	0.004	b.d.	0.006	0.002	b.d.	0
Cd	0.506	0.612	0.414	0.411	b.d.	b.d.	0.042	0.236
Ag	0.002	0.005	0.006	b.d.	0.002	0.007	b.d.	b.d.
Sn	b.d.	0.001	b.d.	b.d.	0.002	b.d.	b.d.	0.008
Co	b.d.	0.004	0.004	0.021	0.037	0.037	b.d.	b.d.
In	b.d.	b.d.	b.d.	b.d.	b.d.	b.d.	b.d.	b.d.
Total	100.72	100.897	98.883	100.83	101.153	101.18	101.018	101.263

2.4.1.2 Zeolites

Clinoptilolite-Ca and heulandite-Ca are found throughout Zone 1 but are in larger amounts at the top. Both in-situ XRD (Figure 10) and Raman (Figure 11) indicate the peaks best match clinoptilolite-Ca and heulandite-Ca.

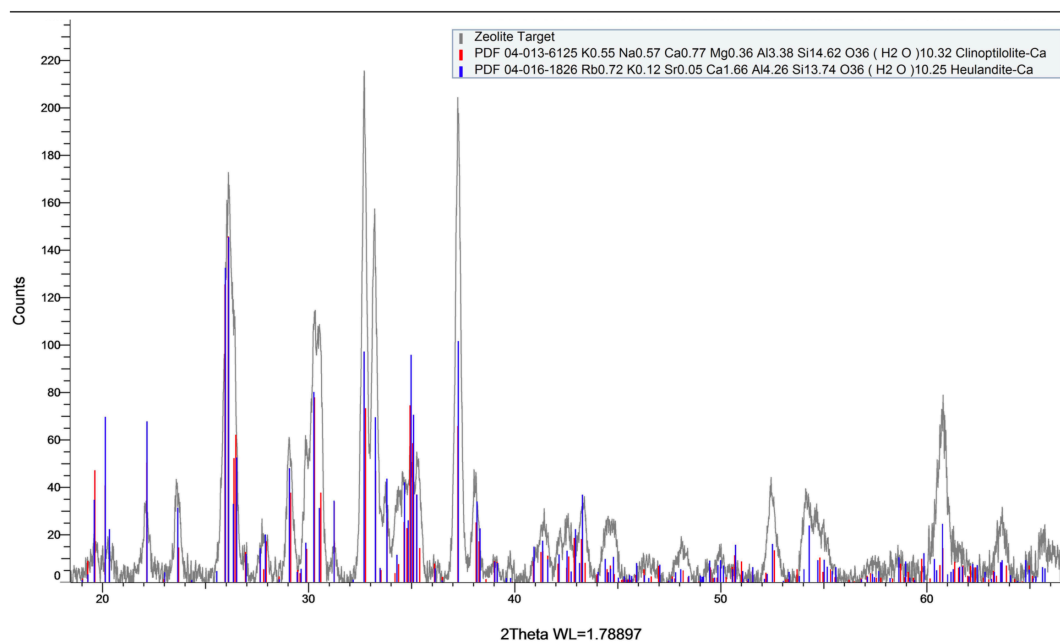


Figure 10: μ XRD of zeolites at 271.2 m depth. XRD scan with both clinoptilolite-Ca and heulandite-Ca for reference.

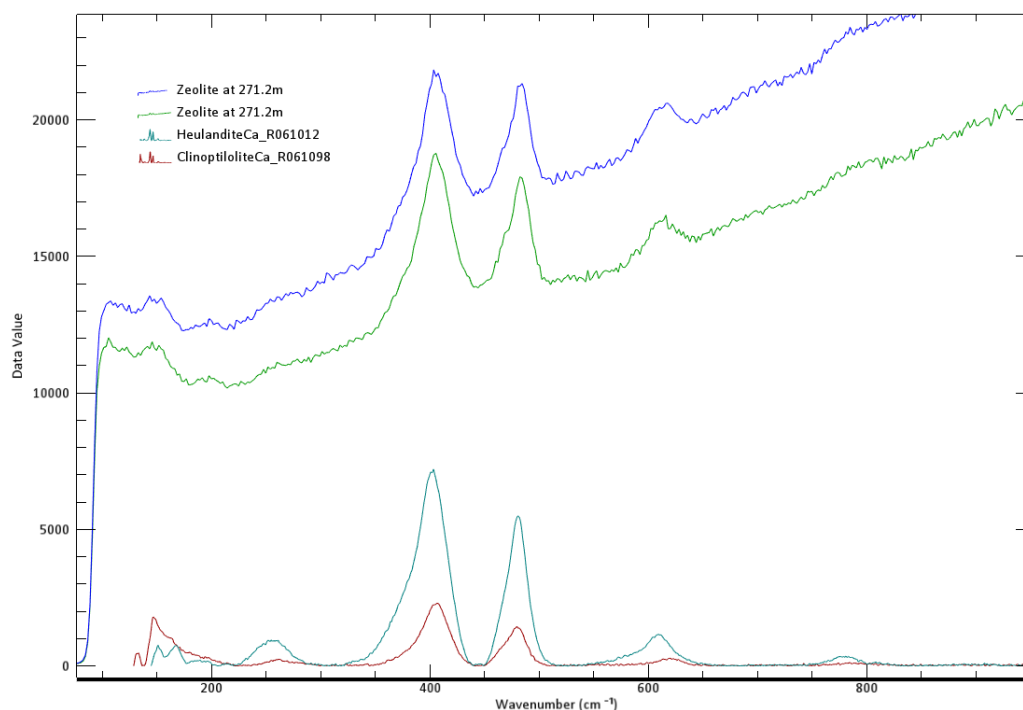
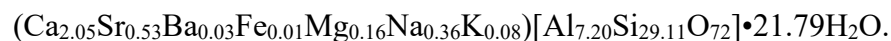


Figure 11: Raman Spectroscopy of zeolites at 271.2 m depth. Measured Raman peaks, closely resembling the signatures of both clinoptilolite-Ca and heulandite-Ca.

After determining that either, or both, clinoptilolite-Ca and heulandite-Ca were present, the minerals were distinguished through EMPA techniques (Table 4, Table 3). Both zeolites occur at the top of the melt sheet in Zone 1. Clinoptilolite-Ca is found as radial, tabular crystals. The crystals radiate out from oxidized material that is from the first sulfide group that is deposited. Radial clinoptilolite-Ca is observed in a few different localities within Zone 1. The highest abundance of zeolites is at 271.2m. The formula calculated from WDS microprobe analysis for the radial clinoptilolite-Ca is:



Heulandite-Ca is found as non-oriented tabular crystals intersected by circular botryoidal features. These features have been found to comprise heulandite-Ca, smectites, and quartz (Figure 12, Figure 14). The formula calculated from microprobe analysis for the botryoidal heulandite-Ca at 271.2 m is:

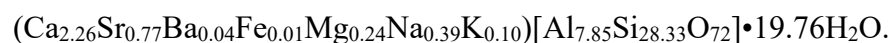


Table 3: Clinoptilolite-Ca and heulandite-Ca in Zone 1. Clinoptilolite-Ca has a $T_{Si} \geq 80$ and an $Si:Al \geq 4$. Heulandite-Ca has a $T_{Si} < 80$ and an $Si:Al < 4$ (Coombs et al., 1997; Coombs et al., 1998).

Depth (m)	Habit	Mineral	T_{Si}	Si:Al
271.2	Radial, tabular	Clinoptilolite-Ca	0.802	4.05
	Botryoidal, tabular	Heulandite-Ca	0.783	3.61
271.6	Rim, poorly defined	Heulandite-Ca	0.792	3.81
	Radial, tabular	Clinoptilolite-Ca	0.813	4.35
	Botryoidal, tabular	Heulandite-Ca	0.770	3.34

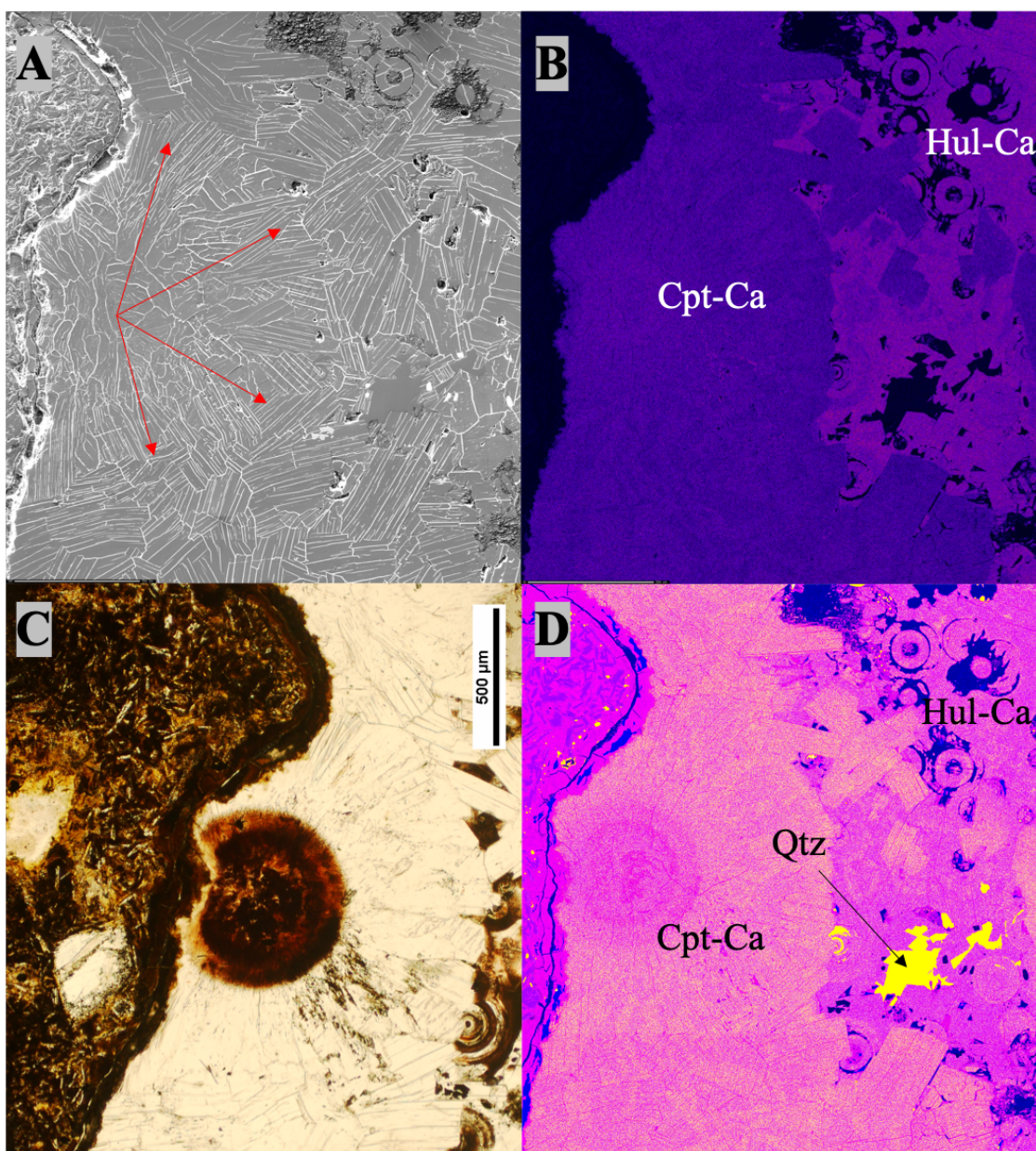


Figure 12: Radial clinoptilolite-Ca (Cpt-Ca) and botryoidal heulandite-Ca (Hul-Ca).

A. Scanning electron image highlights the radial nature, indicated by the red arrows, of the tabular clinoptilolite-Ca. **B.** Element map of strontium. The botryoidal heulandite-Ca contains a higher amount of strontium. **C.** Plane polarized light image centred on the oxidation halo. The oxidation of the nickel-iron sulfides is evident (millerite and vaesite-pyrite) encased in the radial heulandite. **D.** Silica over aluminum element map. The different zeolites are highlighted by Si:Al ratios.

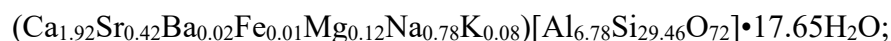
Quartz (Qtz) is highlighted amongst the botryoidal heulandite.

Table 4: Geochemical data from clinoptilolite-Ca and heulandite-Ca in Zone 1 at 271.2 m depth. *H₂O was assumed as the remaining mass (100-total) **Total value not including H₂O.

Mass%	Radial Clinoptilolite				Botryoidal Heulandite				
	1	2	3	4	5	6	7	8	9
SiO ₂	64.593	64.105	64.508	65.549	61.841	63.247	62.894	63.173	64.159
Al ₂ O ₃	14.127	13.804	13.477	12.841	14.652	14.986	15.09	14.839	14.597
FeO	0.032	0.022	0.003	0.019	0.047	0	0.079	0.013	0.04
MgO	0.3	0.206	0.208	0.224	0.32	0.393	0.36	0.379	0.32
CaO	4.225	4.354	4.355	4.052	4.605	4.784	4.653	4.723	4.716
Na ₂ O	0.661	0.424	0.276	0.279	0.234	0.476	0.515	0.51	0.482
K ₂ O	0.111	0.097	0.171	0.182	0.101	0.178	0.207	0.216	0.183
BaO	0.135	0.147	0.161	0.138	0.228	0.224	0.221	0.25	0.242
SrO	2.103	2.132	2.106	1.8	3.039	2.915	3.034	2.878	2.988
Rb ₂ O	nd	nd	nd	nd	nd	nd	nd	nd	nd
Cs ₂ O	nd	nd	0	nd	nd	0.001	nd	nd	nd
P ₂ O ₅	0	nd	nd	0	nd	0.007	nd	0.009	nd
H ₂ O*	13.713	14.709	14.735	14.916	14.933	12.789	12.947	13.01	12.273
Total**	86.287	85.291	85.265	85.084	85.067	87.211	87.053	86.99	87.727

Slightly lower in upper Zone 1 at 271.6 m depth, three different zeolites are observed. Two are similar in character to the ones found at 271.2 m. The third is a heulandite-Ca defined only by geochemical, not crystal boundaries that encases the others, located at the base of the radial clinoptilolite-Ca (Figure 14). The calculated formulas for each are below:

Radial clinoptilolite-Ca:



Botryoidal heulandite-Ca:

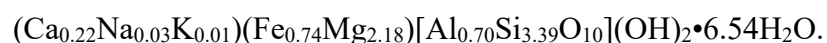


Rim heulandite-Ca:



2.4.1.3 Clays

In-situ XRD analysis revealed that smectites, such as saponite, montmorillonite, and kaolinite, are present at East Clearwater. Saponite at 271.6 m (Figure 14) was calculated from EMPA WDS data to have the chemical formula of:



Clays signatures, specifically smectites, are present mostly in Zone 1, although trace amounts may exist in Zone 2 from ASD spectra (Figure 13).

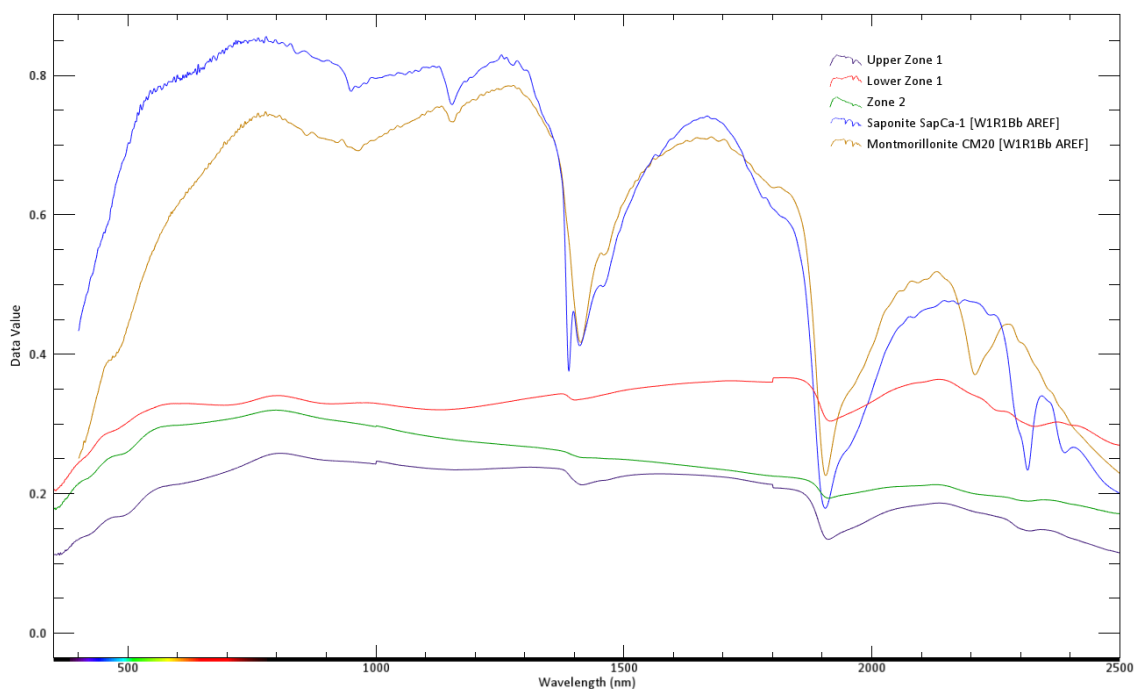


Figure 13: UV-Vis-NIR spectroscopy of Zone 1 and 2 compared to smectites.

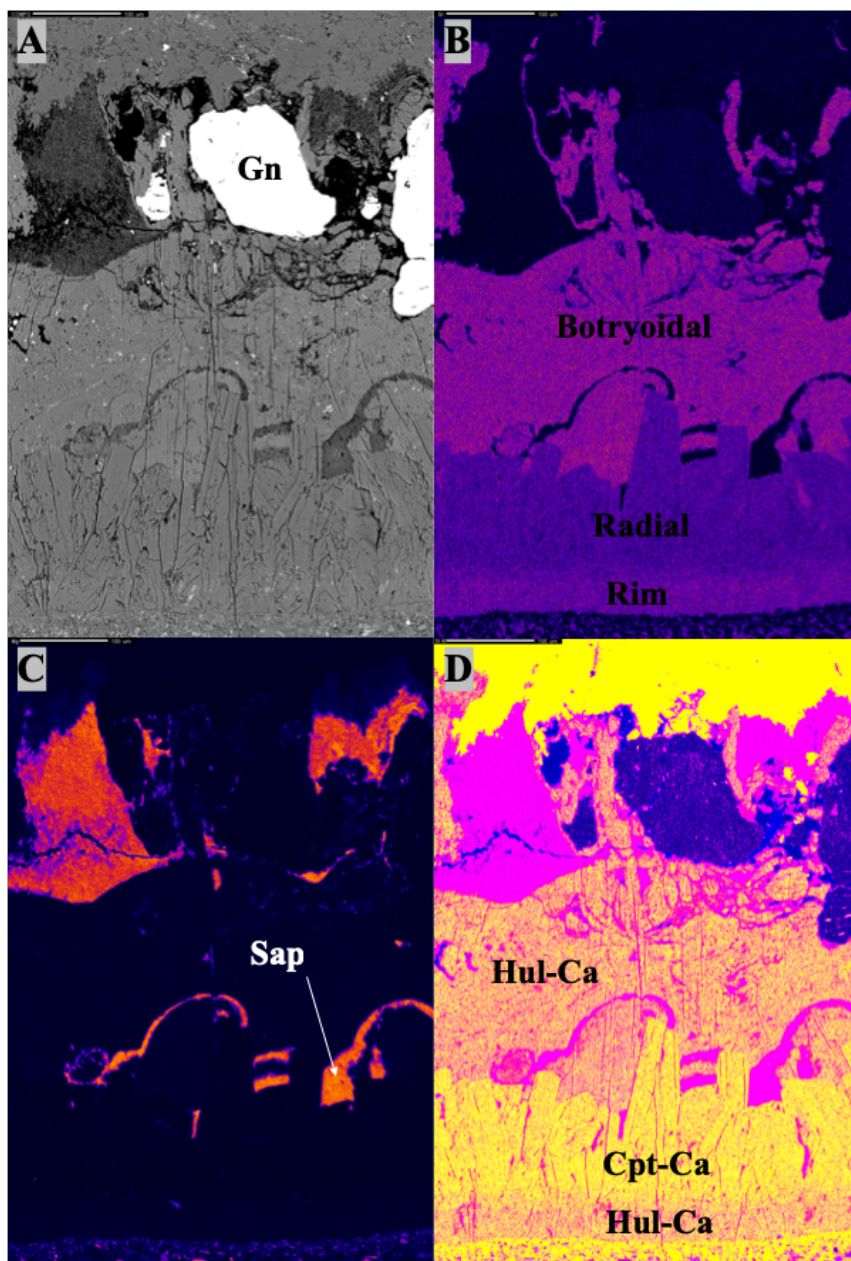


Figure 14: Radial clinoptilolite-Ca (Cpt-Ca), botryoidal heulandite-Ca (Hul-Ca), and rim heulandite-Ca at 271.6 m depth A. Composite image highlighting the presence of galena (Gn) and the structure of the zeolites. B. Elemental map of strontium. Higher concentrations are also apparent in the rim heulandite-Ca. C. Magnesium element map. Mg-rich saponite (Sap) is found in the botryoidal structures surrounded by heulandite-Ca. D. Silica over Aluminum element map. Si:Al highlights the difference between the two zeolites.

2.4.2 Zone 2

Zone 2 (Figure 6C) contains fewer vugs. Many are no larger than a few centimetres filled 70–100% by chlorite, radial quartz, calcite, and sulfides, such as galena, pyrite, and sphalerite, and cassiterite. A few are vugs centimetre- to decimetre- wide filled 100% filled by calcite, with minor quartz and sparse galena, pyrite, and sphalerite (Figure 15). Besides the vugs, a pervasive chloritization is present in the silicate melt, giving the matrix a dark green colour (Figure 6).

2.4.2.1 Chlorite

The chlorite zone of the East Clearwater core contains little to no free space, as most vugs are filled by chlorite and radial quartz (Figure 15). Clinocllore-chamosite is the dominate chlorite present. The formula calculated from WDS microprobe analysis for the clinocllore-chamosite at 290.4 m depth is:



2.4.2.2 Calcite

Calcite exists in vugs with quartz and few sulfides including galena, pyrite, and sphalerite. It is zoned with lighter calcite being more enriched in manganese and iron (Figure 16). Calcite is not found in vugs associated with chlorite and vice versa.

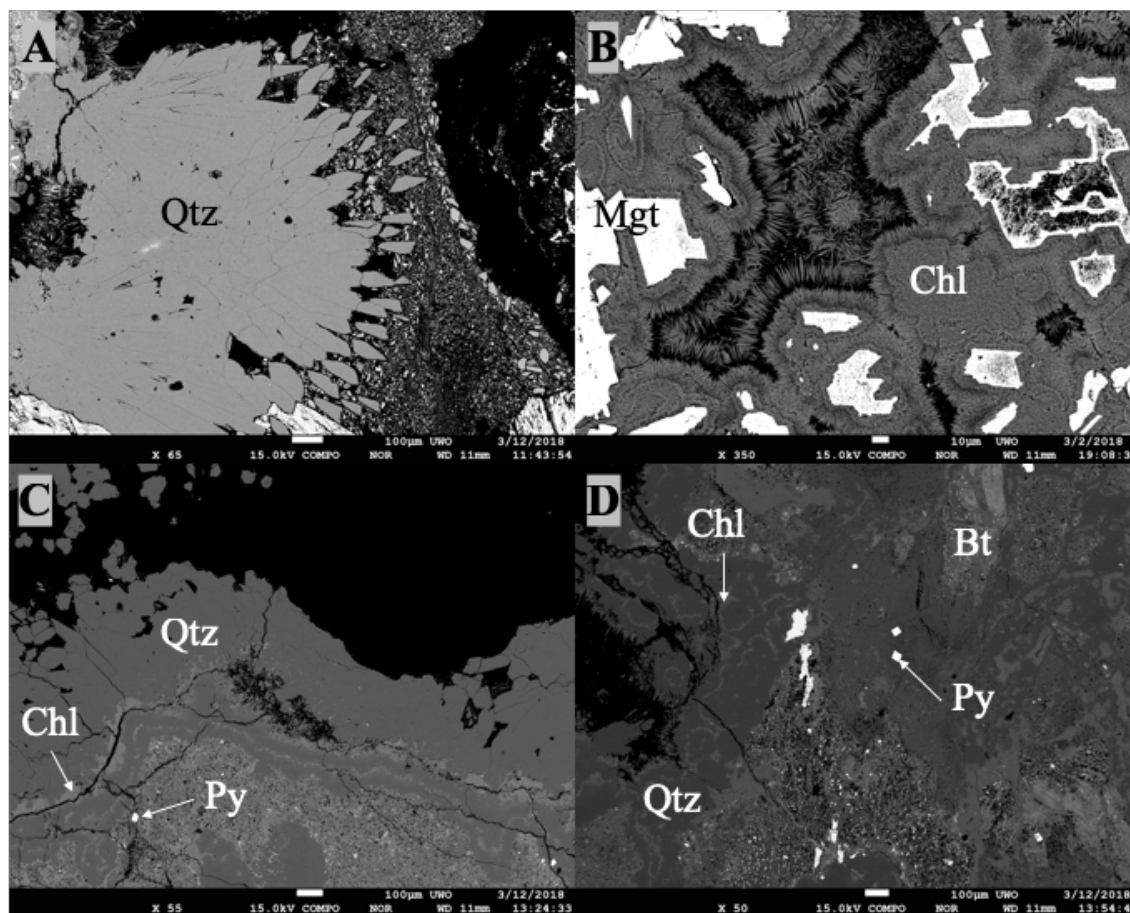


Figure 15: The mineralization style of vugs in the chlorite zone. A) Radial quartz (Qtz) in a vug at 280.1 m depth. B) Chlorite (Chl) infilling vug with magnetite (Mgt) found in a clast at 290.4 m. C & D) Quartz dominated vug with chlorite, biotite (Bt), and pyrite (Py) at 295.3 m.

2.4.2.3 Sulfides

Both the nickel-iron and Pb-Zn-Cu-Fe sulfides as described in Zone 1 are present in Zone 2 in smaller amounts. Primary sulfides show exsolution textures, with some of them containing secondary sulfides nearby. For example, a pentlandite bordering carbonate melt at 308.9 m depth contains exsolved galena with secondary pyrite and sphalerite residing nearby (Figure 16).

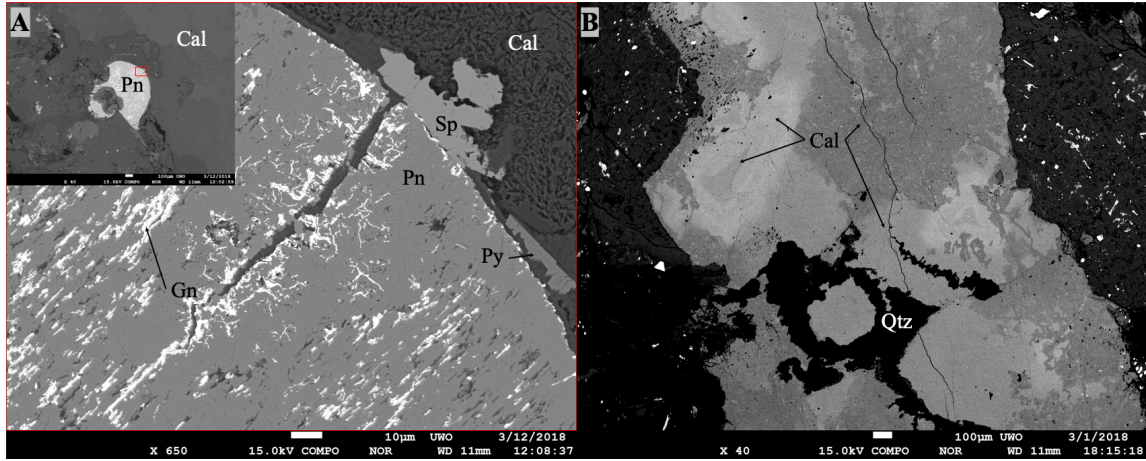


Figure 16: A. Large Pentlandite crystal at 308.9 m depth. Galena (Gn) exsolution in pentlandite (Pn), precipitation of sphalerite (Sp) and pyrite (Py) on the rim. B. Zoned calcite (Cal) with quartz (Qtz). The lighter shades are caused by higher Mn and Fe.

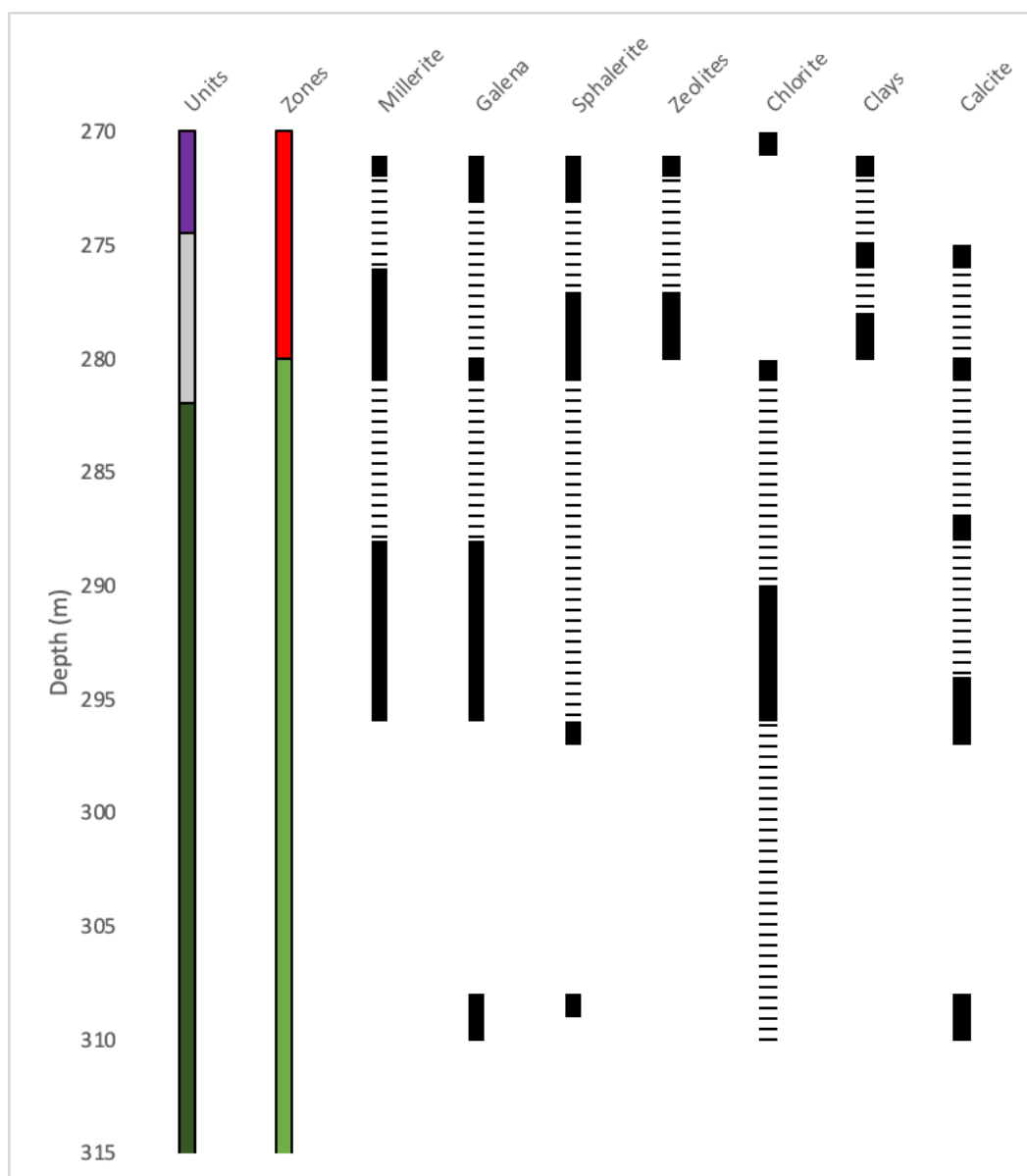


Figure 17: Mineralization with depth in East Clearwater Core 2-63. Black means minerals have been identified. Dashed lines indicate trace amounts. Units from top to bottom: Impact melt-bearing breccia; Vesicular impact melt rock; Fine-grained coherent impact melt rock. Zones from top to bottom: Zone 1; Zone 2. Zones are defined by the transition between the zeolites and clays and the chlorite.

2.5 Discussion

2.5.1 Heat Sources

The majority of the heat for the East Clearwater system at the observed areas would have come from the impact melt sheet itself. Impact craters of similar diameter, e.g., Haughton (24 km) and Ries (~24 km) have structural uplifts of 1–2 km (Osinski et al., 2001; Osinski, 2005). The elevated geotherm provides a maximum temperature of ~40–70 °C assuming a geothermal gradient of 30 °C km⁻¹ and a surface temperature of ~10 °C. While this elevated geotherm may have been more important elsewhere in the crater (such as the central uplift), the heat driving the observations made here would have been from the melt sheet itself. The vertical extent, let alone the volume, of the impact melt rocks and melt-bearing breccias is unknown, as only the top ~46 m of these impactites were recovered (Dence et al., 1965).

2.5.2 Fluid sources

No pre-impact sediments are found as clasts in East Clearwater impact breccias like they are in West Clearwater (Palme et al., 1979). These sediments would have been present during the impact at East Clearwater, but it is likely they were either not formed or not consolidated at the time of impact. East Clearwater impacted into a shallow marine or costal environment of the paleocontinent of Laurentia (Schmieder et al., 2015). It is likely that a major source of the hydrothermal fluids would have come from seawater. This is supported by the observation that there are significant amounts of strontium in both clinoptilolite-Ca and heulandite-Ca. Further isotopic analysis would have to be conducted to determine the source.

2.5.3 Early Stage

The hydrothermal system at East Clearwater precipitated many different minerals as the system matured. The Ni-Fe sulfides of millerite and vaesite-pyrite were some of the first minerals to be deposited. At East Clearwater, the impactor was only partially vaporized with a significant portion being incorporated into the melt, therefore enriching metal content (Grieve et al., 1981). It is likely these siderophile-rich metals were some of the

first materials to be mobilized in the hydrothermal system, which would result in an early stage of secondary sulfide deposition.

2.5.4 Main Stage pH and temperature constraints

Radial clinoptilolite-Ca nucleated from the nickel-iron sulfides. Temperature decreased as clinoptilolite-Ca grew, the nickel-iron sulfides were oxidized, leaving hematite oxidation haloes imprinted in the clinoptilolite-Ca. Pb-Zn-Cu-Fe sulfides primarily composed of galena and sphalerite, with minor chalcopyrite and pyrite deposited along the edges of the radial clinoptilolite-Ca with botryoidal heulandite-Ca, quartz, and smectites.

Observations at Putschez Katunki indicate the increase Si:Al ratio in zeolites and phyllosilicates is caused by an increase in pH with decreasing depth (Donahoe and Liou, 1985; Naumov, 2005). As temperature decreases throughout magmatic-generated hydrothermal systems in granitic rocks, the fluid becomes Na- and Ca- enriched, pH increases, and it becomes more oxidizing all due to mass balancing as chloride complexes dissociate (Dolejš and Wagner, 2008). The majority of the East Clearwater target rocks consist of slightly metamorphosed to relatively undeformed plutonic rocks (Simard et al., 2008), so one may expect a similar fluid trend in an impact-generated hydrothermal system here. A decrease in Si:Al ratios can be seen in individual cavities at East Clearwater. Radial clinoptilolite-Ca was the first zeolite to form on the edge of the vugs, followed by the botryoidal heulandite-Ca. This suggests the pH of the East Clearwater impact-driven hydrothermal system increased not only with depth, but within individual cavities over the progression of the system. A decrease in the Si:Al ratios in zeolites can be caused by 1) a decrease of the Si:Al ratio in the hydrothermal fluid (Lechert, 2001), 2) or an increase in pH (Donahoe and Liou, 1985; Lechert, 2001) in the fluid. The presence of quartz with the botryoidal heulandite-Ca indicates that silica content was still relatively high in the fluid. This may indicate that the Si:Al ratio did not decrease by a significant amount, but rather the increasing pH had more of an effect on the transition between clinoptilolite-Ca and heulandite-Ca.

This can be further constrained as the Pb-Zn-Cu-Fe sulfides grew with botryoidal heulandite-Ca. Chalcopyrite is stable at pH values of less than ~7 and precipitates at temperatures ~200 °C (Reed and Palandri, 2006). As pH increases and temperature decreases, bornite replaces chalcopyrite and CuCl is preferred over chalcopyrite precipitation, respectively (Reed and Palandri, 2006). Sphalerite and galena can precipitate under lower temperature and higher pH conditions. Deeper into the melt sheet (Zone 2) chalcopyrite is absent, while sphalerite and galena are present. As lower in the system retained heat for longer, it is likely conditions were too alkaline or low temperature to form chalcopyrite, although no bornite has been found.

Higher Na:Ca ratios indicate formation at a lower temperature (Senderov and Khitarov, 1970; Naumov, 2005). The Na:Ca ratios remain the same within the zeolites. This would tend to indicate that temperature in the system did not decrease significantly over the time of pH decrease. The porous nature of zeolites and the longevity and proximity of their formation would likely have allowed for cation exchanges to occur. This means that the Na:Ca ratios in the zeolites likely reflect the lower limits of the temperature of formation as it progressively cooled. The transition from a smectite-dominant to chlorite dominant hydrothermal zones is ~200 °C (Kristmannsdottir, 1979). The assemblage of high silica zeolites and dioctahedral smectites is stable <80–130 °C (Rychagov et al., 1993; Naumov, 2005).

The pervasive chloritization of the top of Zone 1 and all of Zone 2 likely occurred during this stage. Interactions between the wall rock and clinoptilolite-Ca post-deposition is likely for the occasional appearance of the poorly-defined rim heulandite-Ca.

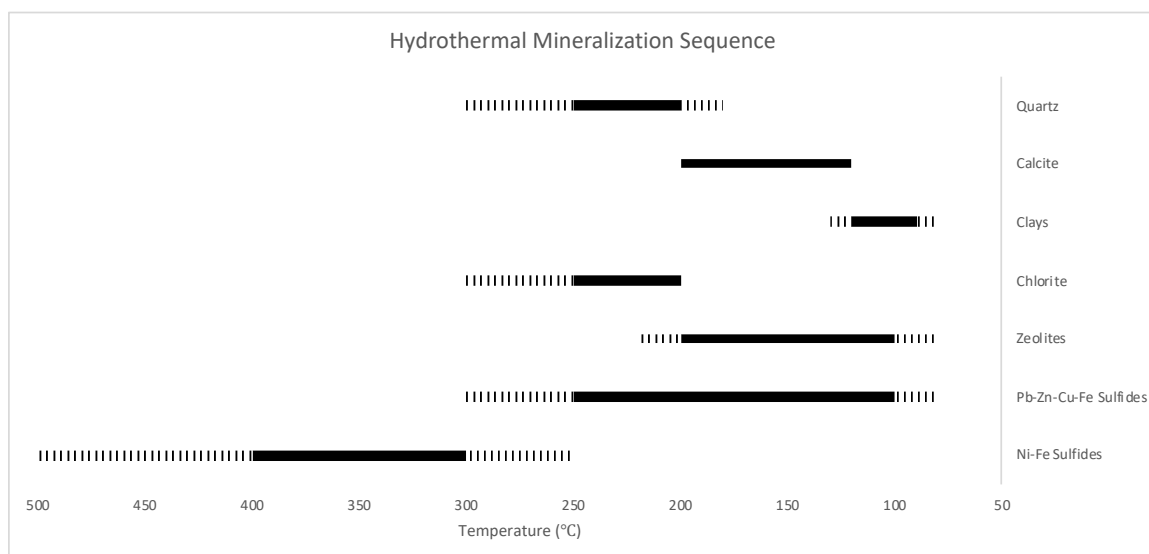


Figure 18: The formation of minerals over the temperature of the East Clearwater hydrothermal system.

2.5.5 Comparison with other impact-generated hydrothermal systems

West Clearwater is directly adjacent East Clearwater at just ~30 km centre to centre, so one might expect similar alteration products. Mg-rich saponitic clays and calcite-dominant vugs have been observed in fine-grained impact melt rock at West Clearwater (Phinney et al., 1978; Kerrigan and Osinski, 2015). These are similar to the saponite and other smectites and calcite vugs observed in this paper at East Clearwater. However, this is where the observed hydrothermal similarities end. The overall alteration style at West Clearwater is very different from the results on East Clearwater reported in this paper. The bright, red rocks of West Clearwater are a stark contrast to the dark green rocks of East Clearwater. In the fine-grained impact melt rock, quartz dominated vugs and calcite dominant vugs have been observed, and in highly vesicular regions, some amygdales (i.e., alteration mineral filled vesicles) have red-to-purple haloes (Kerrigan and Osinski, 2015). A pervasive and partial hematization of many of the impact melt rocks and melt-bearing breccias and veins of pure hematite that are centimetre-scale wide indicates a very oxidative environment. In contrast, oxides found in the melt of East Clearwater have been partially reduced. There is a lack of hydrothermal oxides, with the exception of cassiterite in Zone 2 and hematite from oxidation haloes in Zone 1, although the

oxidation is of the alteration minerals vaesite-pyrite and millerite. The differences in the oxidative/reducing environments is likely due to conditions of impact. Both Clearwater impacts have virtually the same target lithologies (Figure 5), therefore the target rocks are not responsible for the differences in alteration styles between the two craters. The difference in ages, with West and East Clearwater impacted into the Permian (286.2 ± 2.2 Ma) and Ordovician (~460-470 Ma) respectively (Schmieder et al., 2015), it is likely the paleogeological setting that had the largest effect on the styles observed. East Clearwater impacted into a near-coastal to shallow marine environment on the paleocontinent of Laurentia; while West Clearwater impacted into continental Pangea (Schmieder et al., 2015). These paleogeological setting differences suggest that there would have been different sources for hydrothermal fluids. East Clearwater would be affected by seawater, while West Clearwater would be affected by meteoric water and possibly freshwater. As more extensive hydrothermal work is done on West Clearwater, more comparisons and contrast will be made.

The Boltysk impact crater is 25km in diameter and impacted into minor Paleozoic sediments and Precambrian granites and gneisses of the Ukrainian shield at 65.17 ± 0.64 Ma (Kelley and Gurov, 2002; Gurov et al., 2015). This is not a near-coastal or shallow-marine impact like East Clearwater, but similar alteration has been observed here. Boltysk impact breccias contain hydrothermal minerals including K-feldspar, smectites (saponite-nontronite), zeolites (i.e., clinoptilolite), calcite, epidote, garnet, pyrite, and chlorite (Naumov, 2002; Williams, 2012; Williams et al., 2013). Smectite, chlorite, calcite, zeolites, stilpnomelane, sulfides (i.e., pyrite, sphalerite) and elemental metals (copper, silver, platinum, and cuproplatinum) exist in the impact melt rocks (Naumov, 2002; Gurov et al., 2015). The smectites and zeolites are mostly located higher up in the column, while chlorites are below them (Naumov, 2002). A range of native metals is found at Boltysk in the upper unit of the impact melt rocks. They range from copper, silver, platinum, and cuproplatinum. sphalerite, and pyrite They form at the margins of chlorite grains in veins and vein-like structures (Gurov et al., 2015). These zones of alteration are similar to observations on East Clearwater made in this paper (Figure 17). The main alteration differences are K-feldspar, epidote, garnet, and elemental veins have

not been observed at East Clearwater and secondary millerite, vaesite-pyrite, and galena have.

2.5.6 The significance of millerite and vaesite-pyrite

An impactor that is partially incorporated into the melt would influence hydrothermal mineralization, especially with regards to metal oxides and sulfides. Geochemical evidence of an impactor at West Clearwater has not been observed. At East Clearwater, 8% of the melt is impactor derived and nickel is enriched by ~115% according to mixing models using the target rocks and an ordinary chondrite (Grieve et al., 1981). No such nickel enrichment has been observed at West Clearwater (Phinney et al., 1978; Grieve et al., 1981). At Boltysh impact crater, pyrrhotite spheres are present in glassy melt rocks lower in the stratigraphic column, although none are present in the upper impact melt rock unit (Gurov et al., 2015). It is supposed that during the alteration of the upper impact melt rock, pyrrhotite was dissolved into the hydrothermal medium and was a primary source for the secondary elemental metal veins (Gurov et al., 2015). From observations made in this paper, the early availability of nickel and other siderophiles likely provided the nickel to form secondary millerite and vaesite-pyrite.

2.5.7 Conclusions

The East Clearwater hydrothermal system in the impact melt rocks and melt-bearing breccias transitions from zeolite-smectite assemblages to chlorite-dominant assemblages with depth. The pH evolution in impact-generated hydrothermal systems in crystalline targets is similar to magmatic-driven hydrothermal systems in granitic rocks. Given an impact occurs in a water-rich (i.e., non-arid) environment to form a hydrothermal system, the style of alteration will not only vary dependent on target lithologies (i.e., crystalline, sedimentary, mixed target), but also due to on paleogeographic setting (i.e., coastal, shallow marine, intracontinental). The impact-generated hydrothermal system of East Clearwater contains millerite and vaesite-pyrite due to the percentage of impactor imparted into the melt. Given ideal impact velocities do not completely vapourize an impactor, alteration products, especially with regards to metals, can ultimately influence secondary mineralization.

Bibliography

- Beals C. S., Ferguson G. M. and Landau A. (1956) Canadian scientists report (II. A search for analogies between lunar and terrestrial topography on photographs of the Canadian shield, part I. *J. R. Astron. Soc. Can.* **50**, 203–261.
- Bottomley R. J., York D. and Grieve R. A. F. (1990) Argon-40-argon-39 dating of impact craters. In *20th Lunar and Planetary Science Conference Proceedings*. 421–431.
- Commission de toponymie (2016) Lac Wiyâshâkimî. *Gouv. Qué.*
- Coombs D. S., Alberti A., Armbruster T., Artioli G., Colella C., Galli E., Grice J. D., Liebau F., Mandarino J. A. and Minato H. (1998) Recommended nomenclature for zeolite minerals: report of the subcommittee on zeolites of the International Mineralogical Association, Commission on New Minerals and Mineral Names. *Mineral. Mag.* **62**, 533–571.
- Coombs D. S., Alberti A., Armbruster T., Artioli G., Colella C., Galli E., Grice J. D., Liebau F., Minato H., Nickel E. H. and Passaglia E. (1997) Recommended nomenclature for zeolite minerals: Report of the subcommittee on zeolites of the International Mineralogical Association, Commission on New Minerals and Mineral Names. *Can. Mineral.* **35**, 1571–1606.
- Currie K. L. (1971) Origin of igneous rocks associated with shock metamorphism as suggested by geochemical investigations of Canadian Craters. *J. Geophys. Res.* **76**, 5575–5585.
- Dence M. R. (1964) A comparative structural and petrographic study of probable Canadian meteorite craters. *Meteoritics* **2**, 249–270.
- Dence M. R. (1965) The extraterrestrial origin of Canadian craters. *Ann. N. Y. Acad. Sci.* **123**, 941–969.
- Dence M. R., Innes M. J. S. and Beals C. S. (1965) On the probable meteorite origin of the Clearwater Lakes, Quebec. *J. R. Astron. Soc. Can.* **59**, 13–22.
- Dence M. R., Innes M. J. S. and Beals C. S. (1963) On the probable meteorite origin of the Clearwater Lakes, Quebec. *Astron. J.* **68**, 534–535.
- Dolejš D. and Wagner T. (2008) Thermodynamic modeling of non-ideal mineral–fluid equilibria in the system Si–Al–Fe–Mg–Ca–Na–K–H–O–Cl at elevated temperatures and pressures: Implications for hydrothermal mass transfer in granitic rocks. *Geochim. Cosmochim. Acta* **72**, 526–553.
- Donahoe R. J. and Liou J. G. (1985) An experimental study on the process of zeolite formation. *Geochim. Cosmochim. Acta* **49**, 2349–2360.

- Evans N. J., Gregoire D. C., Grieve R. A. F., Goodfellow W. D. and Veizer J. (1993) Use of platinum-group elements for impactor identification: Terrestrial impact craters and Cretaceous-Tertiary boundary. *Geochim. Cosmochim. Acta* **57**, 3737–3748.
- Gill J. E. (1949) Natural divisions of the Canadian Shield. *Trans Roy Soc Can* **43**, 61–69.
- Gosselin C., and Simard M., David J. (2001) *Géologie de la région des lacs des Loups Marins (34A)*., Ressources naturelles, Géologie Québec, Charlesbourg, Québec.
- Grieve R. A. F. (2006) Impact Structures in Canada. *Geological Association of Canada*.
- Grieve R. a. F., Palme H. and Plant A. G. (1981) Siderophile-rich particles in the melt rocks at the E. Clearwater impact structure, Quebec: Their characteristics and relationship to the impacting body. *Contrib. Mineral. Petrol.* **75**, 187–198.
- Gurov E. P., Shekhunova S. B. and Permyakov V. V. (2015) Accessory and opaque minerals in impact melt rocks of the Boltysch structure, Ukraine. *Meteorit. Planet. Sci.* **50**, 1139–1155.
- Kelley S. P. and Gurov E. (2002) Boltysch, another end-Cretaceous impact. *Meteorit. Planet. Sci.* **37**, 1031–1043.
- Kerrigan M. C. and Osinski G. R. (2015) Overview of impact-generated hydrothermal activity at the West Clearwater Lake Impact Structure, Canada. In *46th Lunar and Planetary Science Conference*, 1508.
- Koerberl C., Shukolyukov A. and Lugmair G. W. (2007) Chromium isotopic studies of terrestrial impact craters: Identification of meteoritic components at Bosumtwi, Clearwater East, Lappajärvi, and Rochechouart. *Earth Planet. Sci. Lett.* **256**, 534–546.
- Kristmannsdottir H. (1979) Alteration of Basaltic Rocks by Hydrothermal-Activity at 100-300°C. In *Developments in Sedimentology. Elsevier*, 359–367.
- Landsat 8 (2013) A One-Two Punch. *NASA*.
- Lechert H. (2001) The pH-value and its importance for the crystallization of zeolites. In *Verified Syntheses of Zeolitic Materials. Elsevier*, 33–38.
- Leclair A., Labbé J.-Y., Berclaz A., David J., Lacoste P., Maurice C., Sharma K. N. M. and Simard M. (2006) Government geoscience stimulates mineral exploration in the Superior Province, Northern Québec. *Geosci. Can.* **33**, 16.
- McDonald I. (2002) Clearwater East impact structure: A re-interpretation of the projectile type using new platinum-group element data from meteorites. *Meteorit. Planet. Sci.* **37**, 459–464.

- Naumov M. V. (2002) Impact-generated hydrothermal systems: Data from Popigai, Kara, and Puchezh-Katunki impact structures. In *Impacts in Precambrian shields*. Springer, 117–171.
- Naumov M. V. (2005) Principal features of impact-generated hydrothermal circulation systems: mineralogical and geochemical evidence. *Geofluids* **5**, 165–184.
- Norton D. L. (1984) Theory of Hydrothermal Systems. *Annu. Rev. Earth Planet. Sci.* **12**, 155–177.
- Osinski G. R. (2005) Hydrothermal activity associated with the Ries impact event, Germany. *Geofluids* **5**, 202–220.
- Osinski G. R. (2015) Revisiting the West Clearwater Lake Impact Structure, Canada. In *46th Lunar and Planetary Science Conference*, 1621.
- Osinski G. R., Spray J. G. and Lee P. (2001) Impact-induced hydrothermal activity within the Haughton impact structure, arctic Canada: Generation of a transient, warm, wet oasis. *Meteorit. Planet. Sci.* **36**, 731–745.
- Osinski G. R., Tornabene L. L., Banerjee N. R., Cockell C. S., Flemming R., Izawa M. R. M., McCutcheon J., Parnell J., Preston L. J., Pickersgill A. E., Pontefract A., Sapers H. M. and Southam G. (2013) Impact-generated hydrothermal systems on Earth and Mars. *Icarus* **224**, 347–363.
- Palme H., Göbel E. and Grieve R. A. F. (1979) The distribution of volatile and siderophile elements in the impact melt of East Clearwater/Quebec. In *10th Lunar and Planetary Science Conference Proceedings*, 2465–2492.
- Palme H., Janssens M.-J., Takahashi H., Anders E. and Hertogen J. (1978) Meteoritic material at five large impact craters. *Geochim. Cosmochim. Acta* **42**, 313–323.
- Phinney W. C., Simonds C. H., Cochran A. and McGee P. E. (1978) West Clearwater, Quebec impact structure, part II: petrology. In *9th Lunar and Planetary Science Conference Proceedings* **2**, 2659–2694.
- Reed M. H. and Palandri J. (2006) Sulfide mineral precipitation from hydrothermal fluids. *Rev. Mineral. Geochem.* **61**, 609–631.
- Reimold W. U., Grieve R. A. F. and Palme H. (1981) Rb-Sr dating of the impact melt from East Clearwater, Quebec. *Contrib. Mineral. Petrol.* **76**, 73–76.
- Rychagov S. N., Zhatnuev I. S., Korobov A. D., Kiryukhin V. A. and Glavatskikh S. F. (1993) The Structure of a Hydrothermal System. *Nauka Press*.
- Schmieder M., Schwarz W. H., Trieloff M., Tohver E., Buchner E., Hopp J. and Osinski G. R. (2015) New ⁴⁰Ar/³⁹Ar dating of the Clearwater Lake impact structures

- (Québec, Canada)—Not the binary asteroid impact it seems? *Geochim. Cosmochim. Acta* **148**, 304–324.
- Senderov È. È. and Khitarov N. I. (1970) Zeolites: Their Synthesis and Conditions of Formation in Nature. *Nauka Press*.
- Shukolyukov A. and Lugmair G. W. (2001) Extraterrestrial matter on Earth: Evidence from the Cr isotopes. In *Catastrophic Events and Mass Extinctions: Impacts and Beyond*. *Geological Society of America*, **356**, 3041.
- Simard M. (2008) Lexique stratigraphique des unités archéennes du nord-est de la Province du Supérieur. *Ministère Ressour. Nat. Faune Qué.*
- Simard M., David J., and Gosselin C. (2001) Géologie de la région de Maricourt (SNRC 24D)., *Ministère des ressources naturelles*.
- Simard M., Labbé J. Y., Lacoste P., Leclerc A. and Boily M. (2008) Synthèse du nord-est de la province du Supérieur. *Géologie Québec*.
- Williams F. A. (2012) Variations through the Boltysh Suevites: Glasses, groundmass and hydrothermal minerals. *Meteorit. Planet. Sci. Suppl.* **75**, 5077.
- Williams F. A., Kelley S. P., Gilmour I., Jolley D. W. and Gilmour M. (2013) The Boltysh impact crater, Ukraine: smectites from the crater-fill suevites. In *European Planetary Science Congress* **8**, 305.
- Wilson J. T. (1949) The origin of continents and Precambrian history. *R. Soc. Can. Trans.* **43**, 157–184.

Chapter 3

3 Conclusions

This paper is the first to explore alteration assemblages at East Clearwater and provide insight into the nature of the East Clearwater hydrothermal system. Two zones of alteration assemblages are noted. The first is defined by smectites (i.e., saponite) and zeolites (i.e., heulandite-Ca, clinoptilolite-Ca). The second is defined by chlorite and radial quartz.

Zone 1 contains centimetre- to decimetre- wide vugs. The nickel-iron sulfates millerite and vaesite-pyrite are present in just about every vug in Zone 1. In upper Zone 1, radial clinoptilolite-Ca nucleated off Ni-Fe sulfides as they were oxidized. The radial growth of tabular clinoptilolite-Ca encased red oxidation haloes of hematite. Heulandite-Ca, quartz and smectites formed botryoidal features beyond the radial clinoptilolite-Ca. Pb-Zn-Cu-Fe sulfides of galena, sphalerite, chalcopyrite, and pyrite were precipitated along the radial clinoptilolite-Ca and with botryoidal heulandite-Ca. These vugs are filled 75–100%. In lower Zone 1, millerite exists as centimetre-long needles. The majority of the Ni-Fe sulfides are not encased. A thin layer of zeolites rim the vugs. These vugs are only 5–15% filled. Calcite is generally found in other, much smaller vugs throughout Zone 1. At the top of the impact melt-bearing breccias, chlorite is present in altered glass beads, occasionally surrounding orthoclase, and as a pervasive chloritization is present in the silicate melt of the first, giving the matrix a dark green colour (Figure 6).

Zone 2 contains centimetre-wide vugs filled 70–100% by chlorite, radial quartz, calcite, sulfides such as galena, pyrite, and sphalerite, and cassiterite. Calcite-dominated vugs are centimetre- to decimetre- wide and 100% filled by Mn- and Fe- zoned calcite, with minor quartz, and sparse sulfides of galena, pyrite, and sphalerite. A pervasive chloritization of the silicate melt gives the matrix a dark green colour.

The understanding of the hydrothermal mineralogy at East Clearwater can be improved upon from beyond this paper. Utilizing clay separation techniques to form individual clay powders that are analyzed by XRD is crucial to fully understanding the alteration

assemblages. Stable isotopic work of the clays and zeolites can provide insights into the water source they precipitated from and the temperature of formation.

The similar diameter Boltysh crater impacted into similar crystalline target lithologies as East Clearwater. The Boltysh impact was in an intra-continental setting; whereas, East Clearwater was costal to shallow marine. However, many similarities exist within the hydrothermal systems of both craters, especially with regards to their assemblages, with zones dominated by smectites and zeolites at the top, and others dominated by chlorite lower down in the column.

The paleogeographic setting, composition of the melt (i.e., the mixing of target lithologies and impactor), and the size of the crater (i.e., longevity of the system) greatly influences the hydrothermal mineralization formed at impact craters. The Clearwater Complex provides an excellent example of the effect of paleogeographic settings on alteration style with a controlled setting. The target lithologies of both East and West Clearwater are virtually the same. East Clearwater was dominantly affected by seawater; whereas, West Clearwater was dominantly affected by meteoric water. The other notable differences are that West Clearwater is ~10 km larger in diameter than East Clearwater, and a percentage of the East Clearwater impactor mixed with the melt; whereas, the composition of the meteorite at West Clearwater is unknown. In addition to enhancing the study of East Clearwater hydrothermal mineralization, an in-depth characterization of the hydrothermal alteration at West Clearwater will provide further insights into paleogeological differences.

Curriculum Vitae

Name: Derek King

**Post-secondary
Education and
Degrees:** Carleton University
Ottawa, Ontario, Canada
2011-2015 B.Sc.

The University of Western Ontario
London, Ontario, Canada
2016-present M.Sc.

**Honours and
Awards:** NSERC-CREATE Fellowship
Technologies and Techniques for Earth and Space Exploration
2016

Global Opportunity Award
International Learning
2017

Certificate of Appreciation
CPSX Space Outreach Program
2017

**Related Work
Experience** Teaching Assistant
The University of Western Ontario
2016–2018

Publications:

Osinski, Gordon R. et al. (2018) The CanMars Mars Sample Return analogue mission.
Planetary and Space Science.